AEDC-TR-68-82

AN EMPIRICAL CORRELATION OF PRESSURE ON BLUNT-NOSED CYLINDRICAL AFTERBODIES AT HYPERSONIC MACH NUMBERS

R. H. Eaves, Jr.

ARO, Inc.

May 1968

VON KÁRMÁN GAS DYNAMICS FACILITY
ARNOLD ENGINEERING DEVELOPMENT CENTER
AIR FORCE SYSTEMS COMMAND
ARNOLD AIR FORCE STATION, TENNESSEE

NOTICES

When U. S. Government drawings specifications, or other data are used for any purpose other than a definitely related Government procurement operation, the Government thereby incurs no responsibility nor any obligation whatsoever, and the fact that the Government may have formulated, furnished, or in any way supplied the said drawings, specifications, or other data, is not to be regarded by implication or otherwise, or in any manner licensing the holder or any other person or corporation, or conveying any rights or permission to manufacture, use, or sell any patented invention that may in any way be related thereto.

Qualified users may obtain copies of this report from the Defense Documentation Center.

References to named commercial products in this report are not to be considered in any sense as an endorsement of the product by the United States Air Force or the Government.

AN EMPIRICAL CORRELATION OF PRESSURE ON BLUNT-NOSED CYLINDRICAL AFTERBODIES AT HYPERSONIC MACH NUMBERS

R. H. Eaves, Jr.
ARO, Inc.

AF – AEDC
Arnold AFS Tenn

FOREWORD

The work reported herein was sponsored by the Arnold Engineering Development Center (AEDC), Air Force Systems Command (AFSC), under Program Element 6540223F.

The results of research presented were obtained by ARO, Inc. (a subsidiary of Sverdrup & Parcel and Associates, Inc.), contract operator of AEDC, AFSC, Arnold Air Force Station, Tennessee, under Contract AF40(600)-1200. The work was conducted over the period from January 1961 to December 1966. Applicable projects for this investigation were ARO Project Numbers VT3116, VT2715, and VT2707, and the manuscript was submitted for publication on March 21, 1968.

This work was presented as a thesis to the Graduate Council of the University of Tennessee in partial fulfillment of the requirements for the degree of Master of Science in March 1968.

The author wishes to acknowledge the many persons in the von Kármán Gas Dynamics Facility (VKF), Arnold Engineering Development Center, whose assistance was instrumental in the preparation of this study. The author is particularly indebted to Dr. J. Lukasiewicz, chief of VKF, for providing documentation of previously reported experimental data and numerical solutions and C. H. Lewis, of VKF, for providing a computer program to obtain additional numerical solutions. Thanks are also due to E. E. Edenfield and R. K. Matthews, of VKF, for providing previously unpublished experimental data.

This technical report has been reviewed and is approved.

Donald H. Meyer
Major, USAF
AF Representative, VKF
Directorate of Test

Roy R. Croy, Jr.
Colonel, USAF
Director of Test

ABSTRACT

This study provides a readily solvable correlating equation that accurately predicts the pressure distribution over the afterbodies of various blunt-nosed cylinders at hypersonic Mach numbers. The correlating equation is developed from experimental pressure data on a cylinder with three nose shapes (hemisphere, flat-face, and rounded-shoulder flat-face) at free-stream Mach numbers of 6, 8, and 10. For blunt-nosed cylinders with nose drag coefficients from 0.89 to 1.72, the correlating equation is applicable over an extended experimental range of Mach number from 5.0 to 10.2 for local pressures greater than free-stream pressure. A good correlation is obtained with the method of characteristics solutions for Mach numbers from 5 to 100 for ten nose diameters along the body, but the applicability of the correlating equation beyond the experimental limits has not been demonstrated.

CONTENTS

LIST OF FIGURES

FIGURE PAGE

NOMENCLATURE

C_D	Nose drag coefficient
d	Cylinder diameter, in.
K	Correlation constant, K = 0.053
ℓ	Model length, in.
M_∞	Free-stream Mach number
m	Exponent of correlating equation, see Eq. 8
P	Model pressure, psia
P_s	Model stagnation pressure, psia
P_{SH}	Model shoulder (tangent point) pressure, psia
P_∞	Free-stream pressure, psia
$Re_{\infty,d}$	Free-stream Reynolds number based on cylinder diameter
$\bar{R}$	Correlating parameter, see Eq. 10
s	Distance along model surface measured from model stagnation point, in.
x	Distance along model axis measured from model stagnation point, in.
x_J	Distance along cylinder surface measured from the nose-cylinder junction (tangent point), in.
x'	Model axis translation coordinate, in., see Eq. 4
γ	Ratio of specific heats
Δx	Model axis shift, in., see Eq. 5

CHAPTER I
INTRODUCTION

The flow field around an aerodynamic vehicle in the hypersonic Mach number range is very complex. The designer is confronted with such problems as structural loading, stability, and extreme heating. Since the heating is most severe at the nose and present day cooling techniques preclude the use of a sharp nose, blunt-nosed bodies are normally used. For such bodies a knowledge of the subsonic, transonic and supersonic regions of the flow field is required to completely investigate the flow characteristics. Being able to make a reasonable prediction of the pressure distribution around the vehicle in these flow regimes is of fundamental importance in understanding the problems of the design.

Many methods have been documented for predicting surface pressures at hypersonic Mach numbers. Some of these methods require electronic computers while others require simple hand calculations. Considerable effort has been directed toward obtaining solutions of the subsonic and transonic flow field of a blunt body. The following represents some of the major contributions in these two flow regimes: inverse method suggested by Van Dyke (1,2)[1], modified Newtonian-

[1]Numbers in parentheses refer to similarly numbered references in bibliography.

Prandtl-Meyer theory of Lees and Kubota (3), Belotserkovskii's method as applied by Gold and Holt (4), and the method of Vinckur (5). The methods of Belotserkovskii and Vinokur have had some success for very blunt bodies such as flat-face cylinders.

The commonly used method of characteristics has proven to be very successful in the study of supersonic flow but is sometimes hampered by the lack of supersonic "starting conditions" or the availability of an electronic computer. This summary is restricted to cylindrical bodies of revolution at zero angle of incidence, so that cylinder surface pressures may also be predicted by incorporating the basic equations of blast analogy and small disturbance theory as presented by Lukasiewicz (6) and a modified blast analogy documented by Love (7). However, no one method of solution appears to adequately predict the surface pressures over the cylinder for different nose shapes and hypersonic Mach numbers. This result then dictated the origin of the work that is presented.

The purpose of this thesis is to provide a readily solvable correlating equation that will accurately predict the pressure distribution over various blunted cylindrical afterbodies at hypersonic speeds. The correlating equation is developed from experimental pressure data on a cylinder with three nose shapes (hemisphere, flat-face, and rounded-shoulder flat-face) at free-stream Mach numbers of 6, 8, and 10.

CHAPTER II
APPARATUS

I. WIND TUNNELS

The experimental data reported herein for correlating purposes were obtained in two of the VKF hypersonic wind tunnels:

1. Gas Dynamic Wind Tunnel, Hypersonic (B).
2. Gas Dynamic Wind Tunnel, Hypersonic (C).

These experimental data were obtained by Matthews (8), and a brief description of the data acquisition and procedures is presented.

Hypersonic tunnels B and C are continuous, closed circuit, variable density wind tunnels with axisymmetric contoured nozzles and 50-in.-diam. test sections. These wind tunnels use air as a test gas. Tunnel B operates at nominal Mach numbers of 6 and 8 at reservoir pressures from 20 to 280 psia and from 50 to 900 psia, respectively, at stagnation temperatures up to 1350°R. Tunnel C operates at a nominal Mach number of 10 at reservoir conditions from 200 to 2000 psia and up to 1900°R. The above operating conditions result in free-stream unit Reynolds numbers from 0.30×10^6 to 5.00×10^6 per foot in Tunnel C. Tunnel B and its associated equipment are shown in Figure 1. Details of Tunnel C are similar to those of Tunnel B. By utilizing the test section tank and safety doors the model may be injected into the tunnels for a test run and then retracted for model

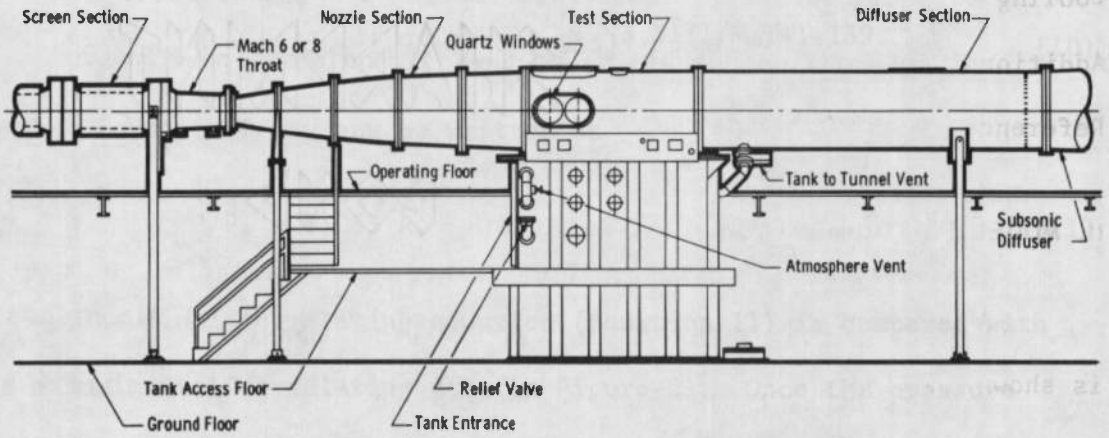

a. Tunnel Assembly

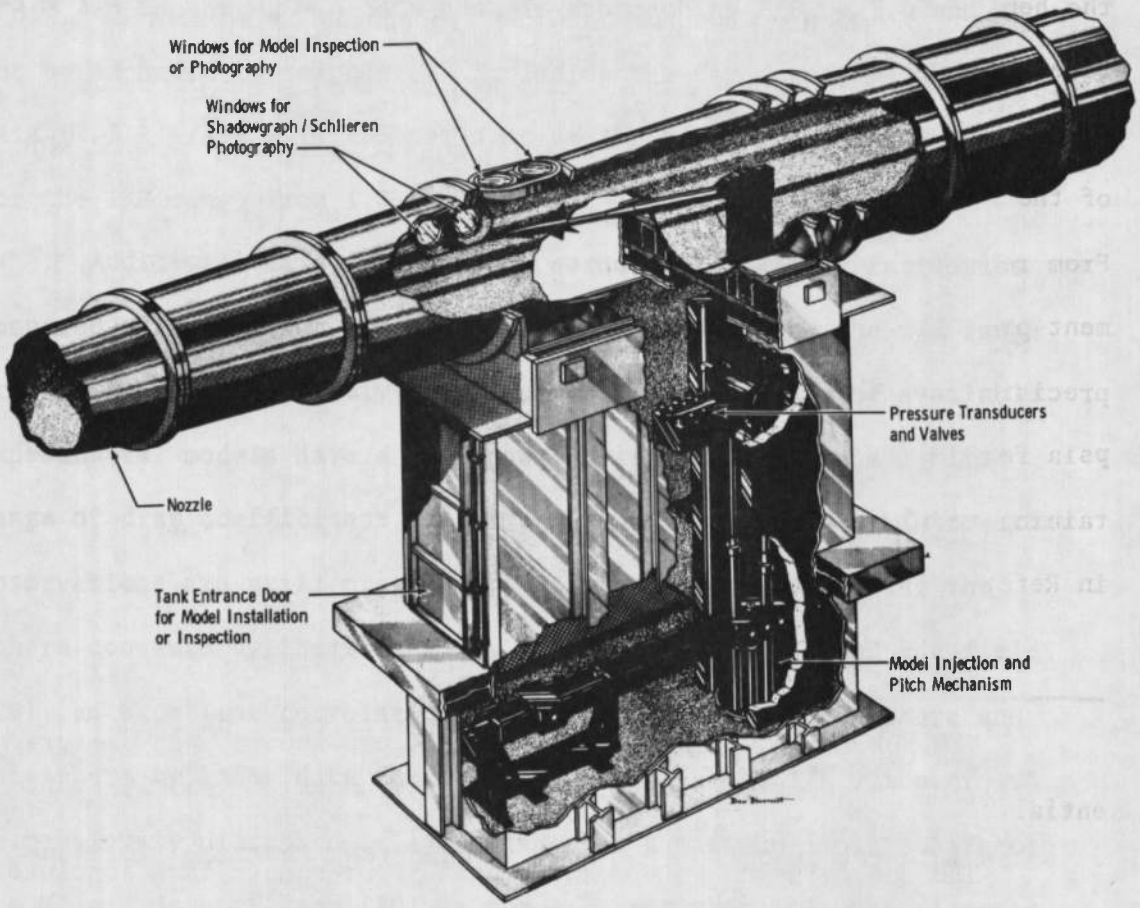

b. Tunnel Test Section

Fig. 1 Tunnel B

cooling or model changes without interrupting the tunnel flow. Additional information pertaining to these tunnels may be found in References 9 through 11.

II. MODELS, INSTRUMENTATION, AND PRECISION

A description of the model geometry and basic model dimensions is shown in Figure 2. The experimental model was a circular cylinder approximately 36 inches long with interchangeable nose configurations. The three nose configurations used to develop the correlation were the hemisphere, flat-face, and rounded-shoulder flat-face. Model surface pressures were measured in Tunnel B with 15-psid[1] transducers and in Tunnel C with 1- and 15-psid transducers, switched in and out of the system automatically to allow measuring to the best precision. From repeated calibrations, the estimated Tunnel B pressure measurement precision was ±0.003 psia.[2] The estimated Tunnel C measurement precision was ±0.001 psia for pressures less than 1 psia and ±0.008 psia for pressures greater than 1 psia. Additional information pertaining to the instrumentation system of Tunnels B and C may be found in References 10 and 11.

---

[1]The abbreviation psid denotes pounds per square inch differential.

[2]The abbreviation psia denotes pounds per square inch absolute.

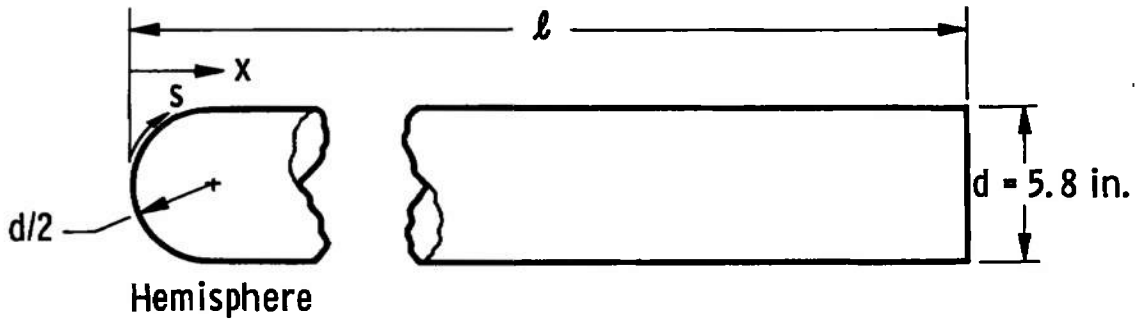

Hemisphere

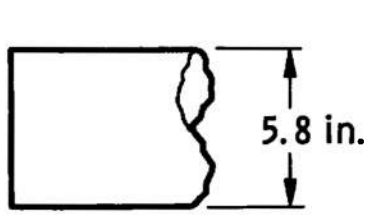

Flat-Face

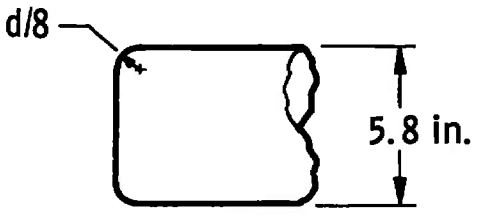

Rounded-Shoulder Flat-Face

		Nose-Cylinder Junction	
Cylinder Nose	ℓ, in.	x/d	s/d
Hemisphere	39.15	0.500	0.785
Flat-Face	35.05	0.000	0.500
Rounded-Shoulder Flat-Face	34.80	0.125	0.570

Fig. 2 Model Geometry

CHAPTER III
TEST CONDITIONS AND PROCEDURES

The test conditions of all experimental data reported herein are summarized in Table I.

Free-stream pitot pressure distributions obtained from tunnel calibrations were used to determine the tunnel axial location at which to position the model. In addition, the symmetry of the model pressure data was usually checked by obtaining data on both the upper and lower model surfaces. The pressure data presented are non-dimensionalized by the model stagnation point value (P_s). Pressure drag coefficients (C_D) of the correlating data were obtained by integrating the pressure data around the nose of the body.

The free-stream conditions were calculated by assuming an isentropic expansion from the stilling chamber to the test section. The ideal gas relationships of Reference 12 were used for Tunnel B (M_∞ = 6 and 8), and to correct for real gas effects, the Beattie-Bridgeman equation of state and the procedures of Reference 13 were used for Tunnel C (M_∞ = 10).

TABLE I
SUMMARY OF TEST CONDITIONS AND DATA SOURCES

Model	d, in.	M_∞	$Re_{\infty,d} \times 10^{-6}$	C_D	Test Gas	Source	Reference
Hemisphere Cylinder	5.8	6	1.0 - 2.16	0.89*	Air	Matthews, AEDC-VKF(B)	8
	5.8	8	0.57 - 1.11	0.89*	Air	Matthews, AEDC-VKF(B)	
	5.8	10	0.34 - 1.15	0.90*	Air	Matthews, AEDC-VKF(C)	
	4.0	≈19.2	≈0.032	0.91⊛	Nitrogen	Matthews, AEDC-VKF(F)	
	1.0	≈18.9	≈0.013	0.91⊛	Nitrogen	Matthews, AEDC-VKF(H)	
	5.8	4 - 8	1.28 - 2.96	0.87 - 0.90x	Air	Baer, AEDC-VKF	30
	3.0	6.87	1.0	0.91+	Air	Crawford and McCauley, Langley 11-in.	32
	0.75	7.7	0.13	0.91+	Air	Lees and Kubota, Galcit Tunnel	3
	---	6.83	0.27 - 0.36	0.91+	Air	Bertram and Henderson, Langley 11-in.	31
	---	9.6	0.06 - 0.11	0.91+	Air	Bertram and Henderson, Langley 11-in.	31
Flat-Face Cylinder	5.8	6	0.97 - 2.12	1.68*	Air	Matthews, AEDC-VKF(B)	8
	5.8	8	0.58 - 1.13	1.70*	Air	Matthews, AEDC-VKF(B)	
	5.8	10	0.34 - 1.16	1.72*	Air	Matthews, AEDC-VKF(C)	
Rounded-Shoulder Flat-Face Cylinder	5.8	6	1.0 - 2.16	1.33*	Air	Matthews, AEDC-VKF(B)	8
	5.8	8	0.58 - 1.13	1.35*	Air	Matthews, AEDC-VKF(B)	
	5.8	10	0.34 - 1.16	1.37*	Air	Matthews, AEDC-VKF(C)	
Sphere-Cone-Arc Cylinder	4.0	8.08	0.5 - 1.0	0.5⊞	Air	Gray, AEDC-VKF(B)	28
	4.0	≈19.3	≈0.076	0.5⊞	Nitrogen	Gray, AEDC-VKF(H)	28
	6.27	≈17.9	≈0.38	0.5⊞	Nitrogen	Edenfield, AEDC-VKF(F)	29
Cut-Sphere Cylinder	5.8	8	0.47 - 1.74	1.51*	Air	Matthews, AEDC-VKF(B)	33

* Integrated Pressure Drag
⊛ Integrated Pressure Drag from $M_\infty \approx 19.2$ Data
⊞ Integrated Pressure Drag from $M_\infty \approx 8.08$ Data
x Integrated Pressure Drag (see Figure 22)
\+ Modified Newtonian

CHAPTER IV
THEORIES FOR PREDICTING CYLINDER PRESSURES

Several theories are investigated to determine if the results are in good agreement with all the experimental surface pressures of the blunt, stream aligned cylinders considered herein. The theories considered are blast analogy by Lukasiewicz (6), modified blast analogy by Love (7), and characteristics theory as applied by Van Hise (14) for sharp-nosed bodies and by Inouye, Rakich, and Lomax (15) for spherically blunt bodies. These methods are briefly discussed before the results are compared with experiment. The theories used herein are based on a ratio of specific heats of 1.4 and nominal free-stream Mach numbers unless otherwise noted.

I. BLAST ANALOGY

Approximate solutions based on blast analogy have been a common approach to the study of hypersonic flows by many workers. Taylor's original solution (16) (first approximation) of a spherical blast was extended by Lin (17) to the case of a cylindrical blast. At approximately the same time, Sakurai (18,19) published first and second approximation solutions of plane, cylindrical, and spherical blasts. Lukasiewicz (6) then derived approximate solutions for predicting the pressure distributions and shock shapes for two-dimensional and axisymmetric flow and compared the results with theoretical calculations

and experimental results. The basic premise of blast analogy is that a sudden, concentrated energy addition to the flow by a blunt-nosed body at hypersonic speeds may be regarded as analogous to an explosive release of energy. By utilizing this analogy and hypersonic small disturbance theory, Lukasiewicz (6) developed a second approximation equation for the pressure distribution which is

$$P/P_\infty = 0.067 \frac{M_\infty^2 C_D^{0.5}}{x/d} + 0.44. \quad (1)$$

For the work reported herein the blast analogy is presented in terms of P/P_s by multiplying Equation 1 by P_∞/P_s at the appropriate free-stream Mach number. The deficiencies of blast analogy in predicting the pressure on cylindrical afterbodies are in the region of the nose-cylinder junction and far downstream ($P/P_\infty < 1.0$). As noted by Lukasiewicz (6), blast analogy should not apply in these two regions because the assumptions of the small disturbance theory are violated. Blast analogy results are compared with the basic experimental data of the hemisphere, flat-face, and rounded-shoulder flat-face cylinders reported herein.

II. MODIFIED BLAST ANALOGY

Many different attempts and suggestions have been made to modify the blast analogy theory to correct the previously mentioned problem areas. This thesis will refer to the work documented by Love (7) as "modified blast analogy". Love adopted the blast wave pressure decay

laws (20) and matched the decay equations with the shoulder pressure (P_{SH}) at the junction of the nose and cylinder ($x_J = 0$). To cope with the downstream problem, the value of P/P_s at $x_J/d = \infty$ was taken to be P_∞/P_s which agrees with characteristics solutions. Love notes that his method is intended primarily for rounded blunting but may be suited for other forms of bluntness. Love's equation is

$$P/P_s = \left[\frac{1}{1 + \left(\frac{x_J}{d}\right)}\right]\left(\frac{P_{SH}}{P_s}\right) + \left[\frac{1}{1 + \frac{1}{\left(\frac{x_J}{d}\right)}}\right]^{P_{SH}/P_\infty}\left(\frac{P_\infty}{P_s}\right). \qquad (2)$$

The pressure decreases from a known value of P_{SH}/P_s toward the free-stream static pressure ratio, P_∞/P_s, as the axial distance (x_J) increases.

An obvious drawback in applying Equation 2 is obtaining satisfactory values of the shoulder pressure ratio (P_{SH}/P_s) for different geometry shapes and Mach numbers. Love (7) examined the hemisphere cylinder and suggested P_{SH}/P_s equal 0.045 for hypersonic Mach numbers, which is in agreement with most of the present experimental data and will be used in this thesis. Clark (21) developed an empirical equation from hemisphere cylinder data for predicting the shoulder pressure over a Mach number range of 2-19 at various Reynolds numbers which differs 18 per cent at Mach 6 from Love's suggested value. Therefore, Clark's predicted value is difficult to use in Love's equation because the cylinder junction pressure is highly sensitive to Reynolds number.

The application of Love's equation to a flat-face cylinder is not feasible, since the overexpanded pressure may vary by two orders of magnitude around the sharp corner. Therefore, since the shoulder pressure cannot be predicted, Love's equation is not used for flat-face cylinder predictions.

Although the rounded-shoulder flat-face cylinder is highly blunted, a well defined experimental shoulder pressure at the junction of the nose and cylinder does exist. From the present rounded-shoulder flat-face data a value of $P_{SH}/P_s = 0.045$ is obtained for Mach numbers 6, 8, and 10 and is used in conjunction with Love's equation for afterbody pressure predictions.

III. CHARACTERISTICS THEORY

When using characteristics solution results to predict the pressure on any geometric body, supersonic "starting conditions" are required to initiate the calculation. The method of obtaining these starting conditions is usually dictated by the nose geometry of the body under consideration. Two specific cases are considered for the work reported herein, namely, a pointed nose cylinder and a spherical nose cylinder.

For the first case, a pointed nose cylinder, Van Hise (14) obtained characteristics solutions for a large number of sharp nosed bodies over a wide range of Mach numbers and drag coefficients. Most of the nose configurations have a small, sharp, tangent cone for initiating the supersonic starting conditions. The calculations of

Van Hise are included to study body shape, drag, and Mach number effects on the final correlating equation. Van Hise correlated his characteristics solutions with the blast wave correlation parameter, $\frac{M_\infty^2 C_D^{0.5}}{x/d}$, and determined the following equation

$$P/P_\infty = 0.060 \frac{M_\infty^2 C_D^{0.5}}{x/d} + 0.55. \quad (3)$$

Equation 3 will not be included for comparison, because the results are similar to the blast wave prediction of Equation 1 with the same previously mentioned deficiencies.

The second case, a spherical nose cylinder, is any body with a spherical nose or a spherical nose with additional nose sections attached to a circular cylinder. Calculations of the subsonic and transonic flow around a blunt body may sometimes be obtained by the inverse method suggested by Van Dyke (1,2) and matched with the characteristics solution at some low supersonic Mach number. The blunt body calculations for the inverse method of Van Dyke are initiated by assuming a shock shape with given free-stream conditions and numerically integrating by a marching technique the flow equations from the shock to the body. An iteration is made on the shock shape until the body shape producing the assumed shock is determined.

As noted by Vaglio-Laurin and Ferri (22), a basic weakness of the inverse method seems to be that shock shapes which are barely distinguishable from each other can lead to radically different body shapes.

The inverse method of Van Dyke and characteristics theory will be referred to collectively in this thesis as the "method of characteristics". The calculations were performed on an electronic computer with a computer program similar to the one of Inouye, Rakich, and Lomax (15).

CHAPTER V
RESULTS AND DISCUSSION

This chapter contains the need and procedure of the present correlation and compares the correlation over a wide range of Mach numbers and nose drag coefficients with additional available experimental data and characteristics theory.

Afterbody pressure distributions of hemisphere, flat-face, and rounded-shoulder flat-face cylinders are correlated for nominal free-stream Mach numbers of 6, 8, and 10. It should be noted here that all the data used for the correlation are at a very high free-stream Reynolds number, $0.34 \leq Re_{\infty,d} \times 10^{-6} \leq 2.16$, where viscous effects are shown to be negligible.

I. NEED FOR AN EXPERIMENTAL CORRELATING EQUATION

The need of a readily solvable equation to predict the afterbody pressure distribution on blunt cylinders at hypersonic Mach numbers will be demonstrated. This will be done by comparing the results of blast analogy, modified blast analogy, and characteristics theory with experimental pressure data on hemisphere, flat-face, and rounded-shoulder flat-face cylinders.

Hemisphere cylinder. If one has an electronic computer and a computer program such as that presented in Reference 15, the results obtained from a characteristics solution are in good agreement with

the hemisphere cylinder pressure distribution at Mach numbers 6, 8, and 10 as illustrated in Figures 3 through 5. This procedure has not been proven for other blunt-nosed cylinders with nose drag coefficients greater than 0.9.

The results of blast analogy (Equation 1) and modified blast analogy (Equation 2) are also compared with the hemisphere cylinder data. Note the obvious inadequate regions of the blast analogy as previously mentioned in Chapter IV. For $s/d < 3.0$ and far downstream ($P/P_\infty < 1.0$) the blast analogy is in poor agreement since the small disturbance theory assumptions are violated as pointed out by Lukasiewicz (6).

The results of Love's modified blast analogy (Equation 2), empirically matched at the shoulder and far downstream are as much as 25 per cent below the hemisphere cylinder data in some regions (Figure 5, page 19, $s/d \approx 4.0$). According to Love (7), the hemisphere cylinder should be the best suited geometry for Equation 2. Figure 3 at Mach number 6 illustrates how critical the choice of P_{SH}/P_s is when applying Equation 2. Two shoulder pressure ratios are assumed, namely, Love's value of 0.045 and Clark's value of 0.053. Although Clark's value of 0.053 will give better agreement with the measured cylinder pressures, it is 7 per cent higher than the present experimental shoulder pressure ratio. Also presented, as with all the experimental data reported herein, are free-stream static pressure ratios (P/P_∞) at each Mach number, determined from the normal shock relations of Reference 12. These ratios represent another reference

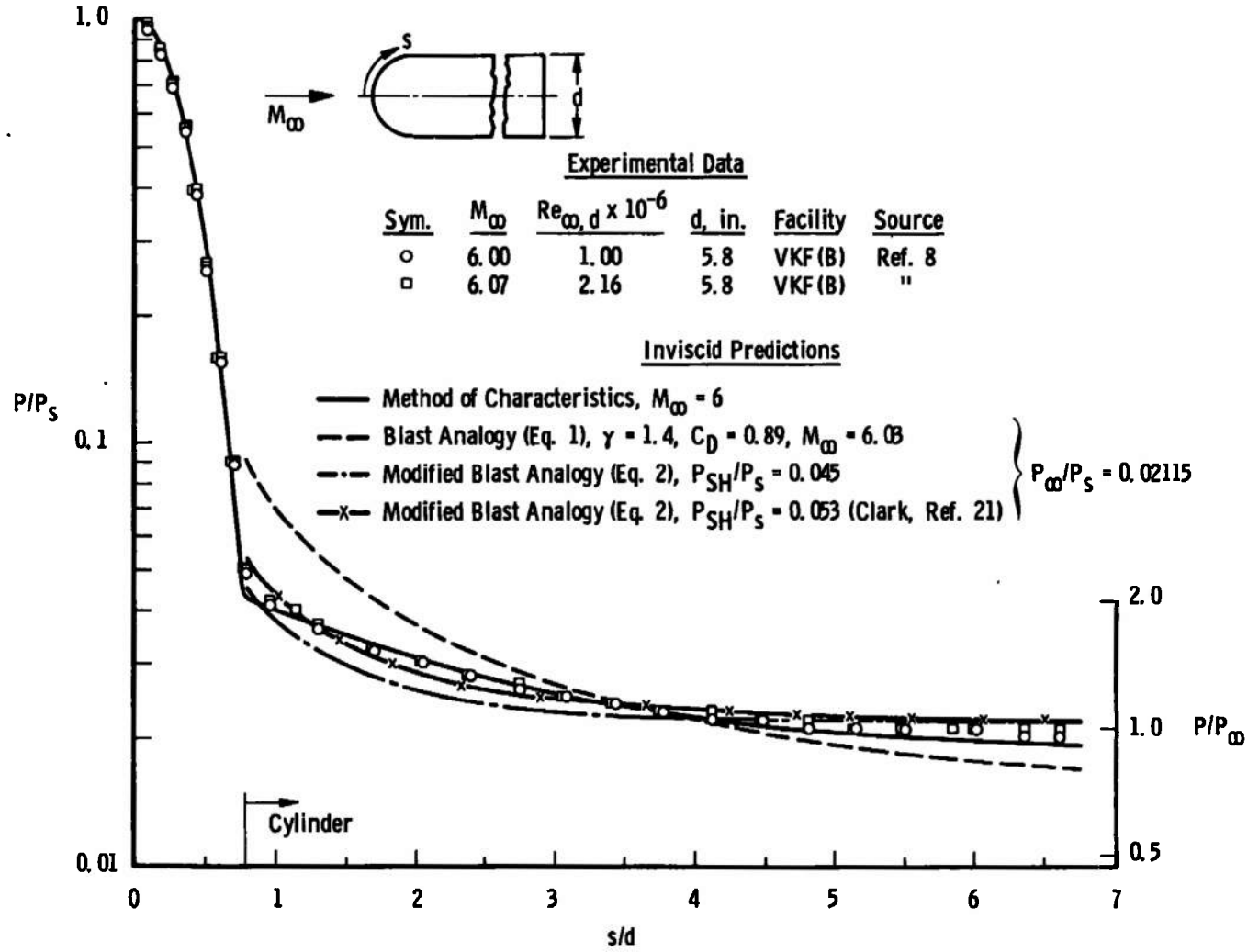

Fig. 3 Experimental and Theoretical Pressure Distributions on a Hemisphere Cylinder at Mach Number 6

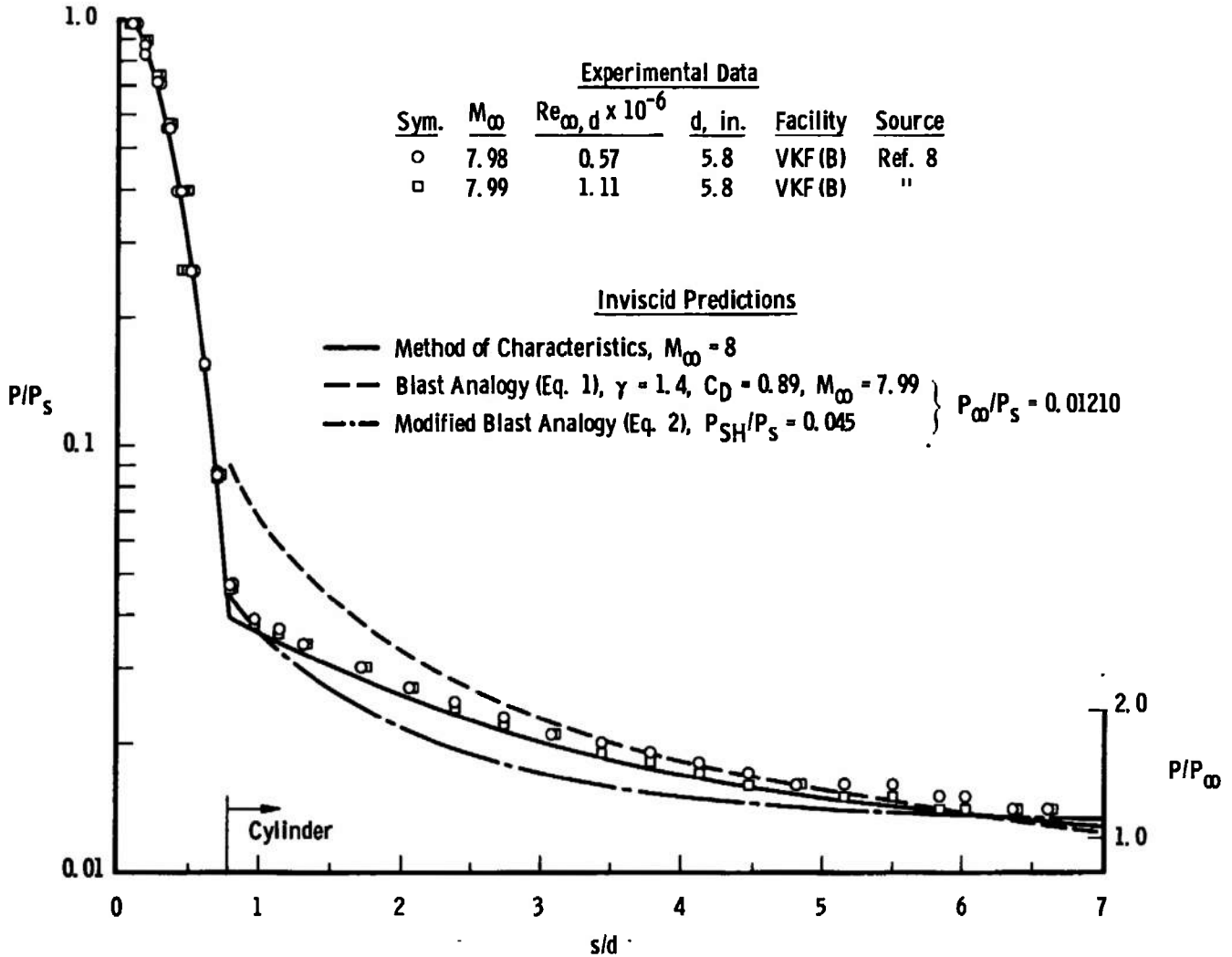

Fig. 4 Experimental and Theoretical Pressure Distributions on a Hemisphere Cylinder at Mach Number 8

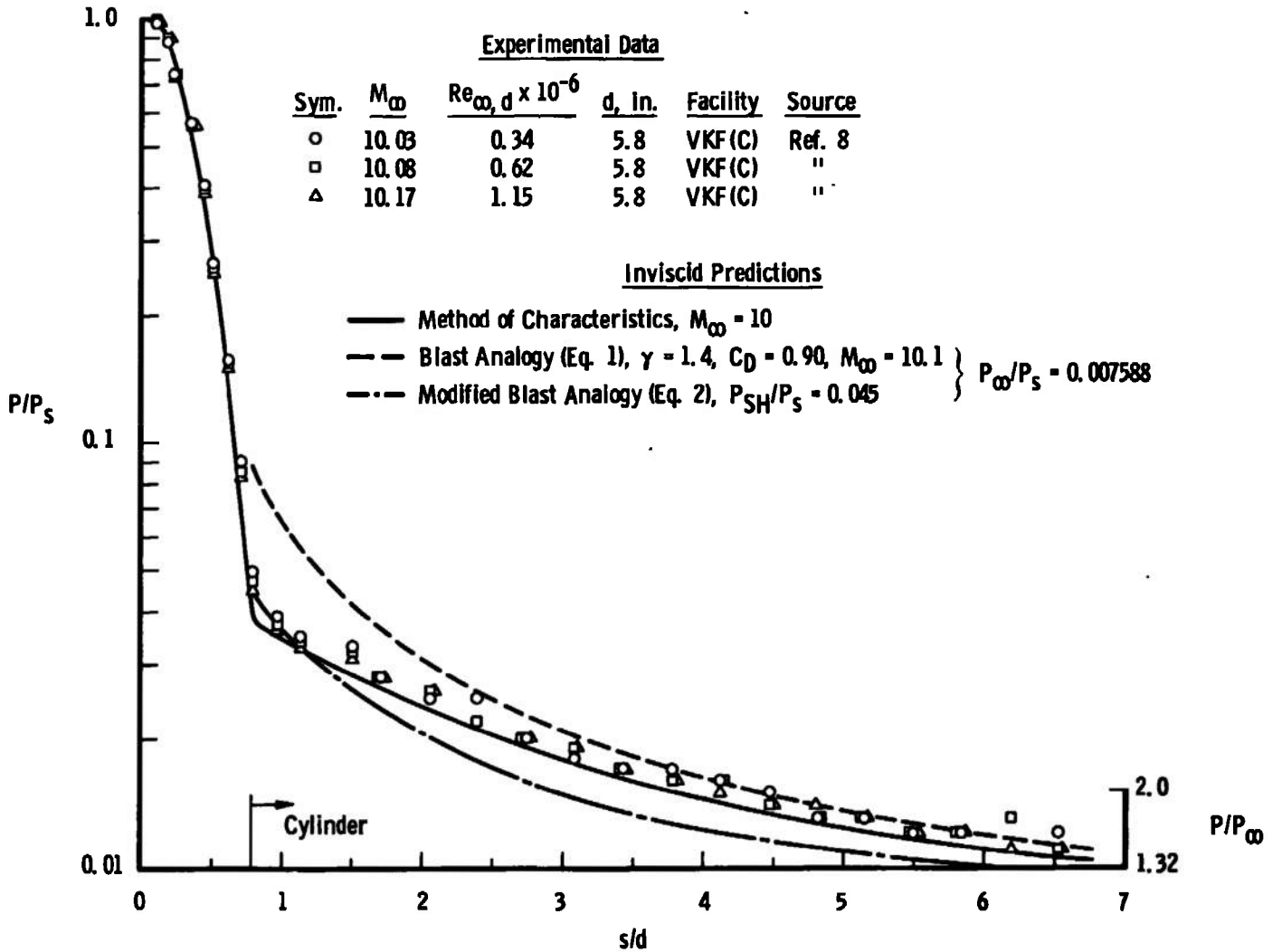

Fig. 5 Experimental and Theoretical Pressure Distributions on a Hemisphere Cylinder at Mach Number 10

level for the experimental pressures presented.

Flat-face cylinder. The flat-face cylinder experimental data at Mach numbers 6, 8, and 10 are presented in Figures 6 through 8. Only blast analogy results are compared here, since it is difficult to apply another theory to this type of geometry (see discussion in Chapter IV).

As previously mentioned, the overexpansion of the pressure around the sharp corner prevents one from determining an appropriate shoulder pressure ratio (P_{SH}/P_s) in applying Love's equation.

Ninety-five per cent of the data is within ±10 per cent of the blast analogy results for s/d greater than 2.5. Observed again is the poor agreement in the nose region similar to the results of the hemisphere cylinder comparison.

Rounded-shoulder flat-face cylinder. The results of Equation 1 (blast analogy) and Equation 2 (modified blast analogy) are compared with the rounded-shoulder flat-face cylinder pressure data and are shown in Figures 9 through 11, pages 24 through 26. Again 95 per cent of the data for s/d greater than 2.5 is within ±10 per cent of the blast analogy results. For s/d less than 2.5 the blast analogy results compare poorly as the previously presented configurations (hemisphere and flat-face cylinders).

Even though a well defined shoulder pressure ratio exists, it exists in an overexpanded pressure region for Mach numbers 6, 8, and 10. Consequently, Love's prediction (Equation 2) underpredicts the pressure level as much as 45 per cent while the experimental pressure

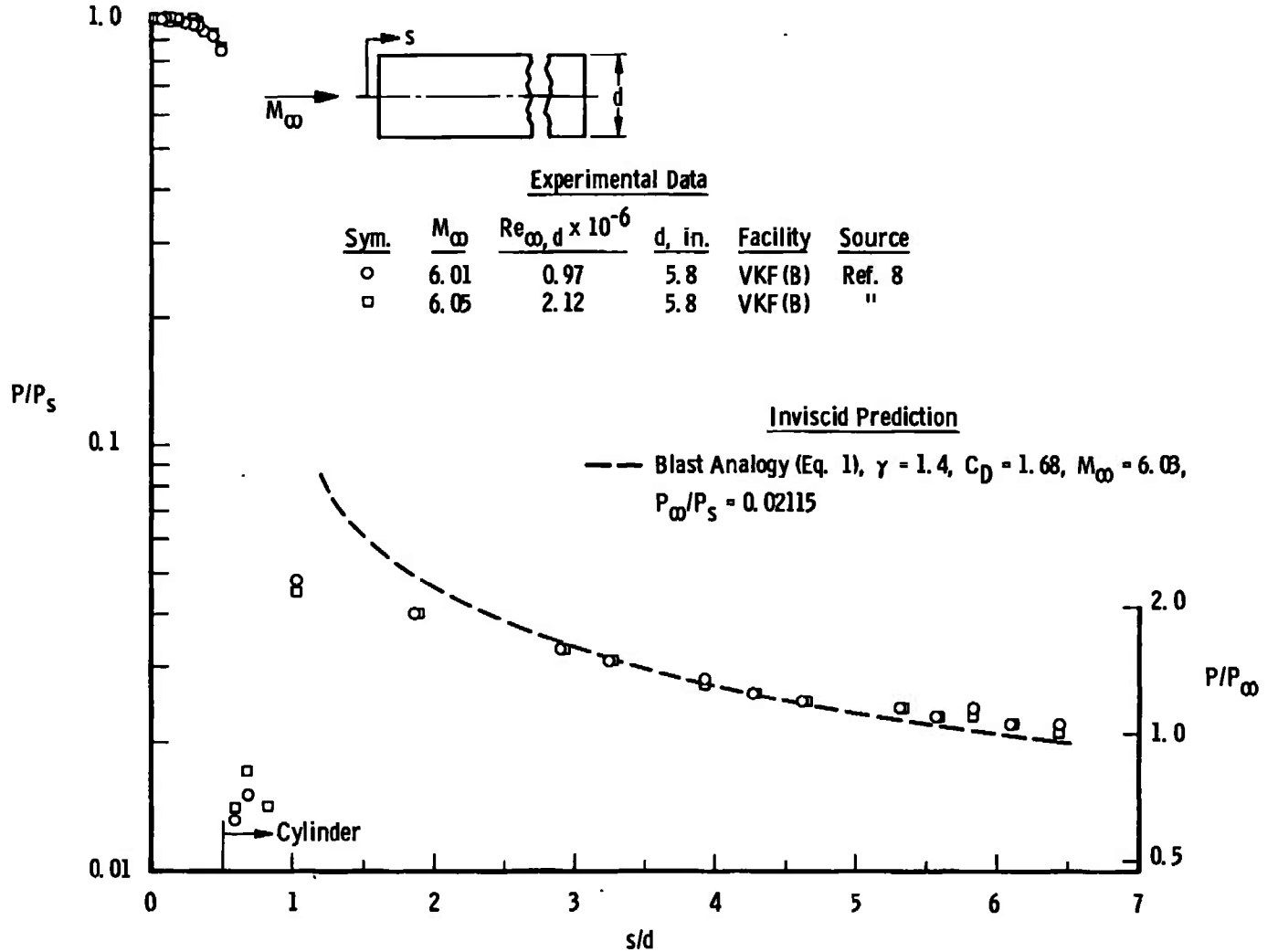

Fig. 6 Experimental and Theoretical Pressure Distributions on a Flat-Face Cylinder at Mach Number 6

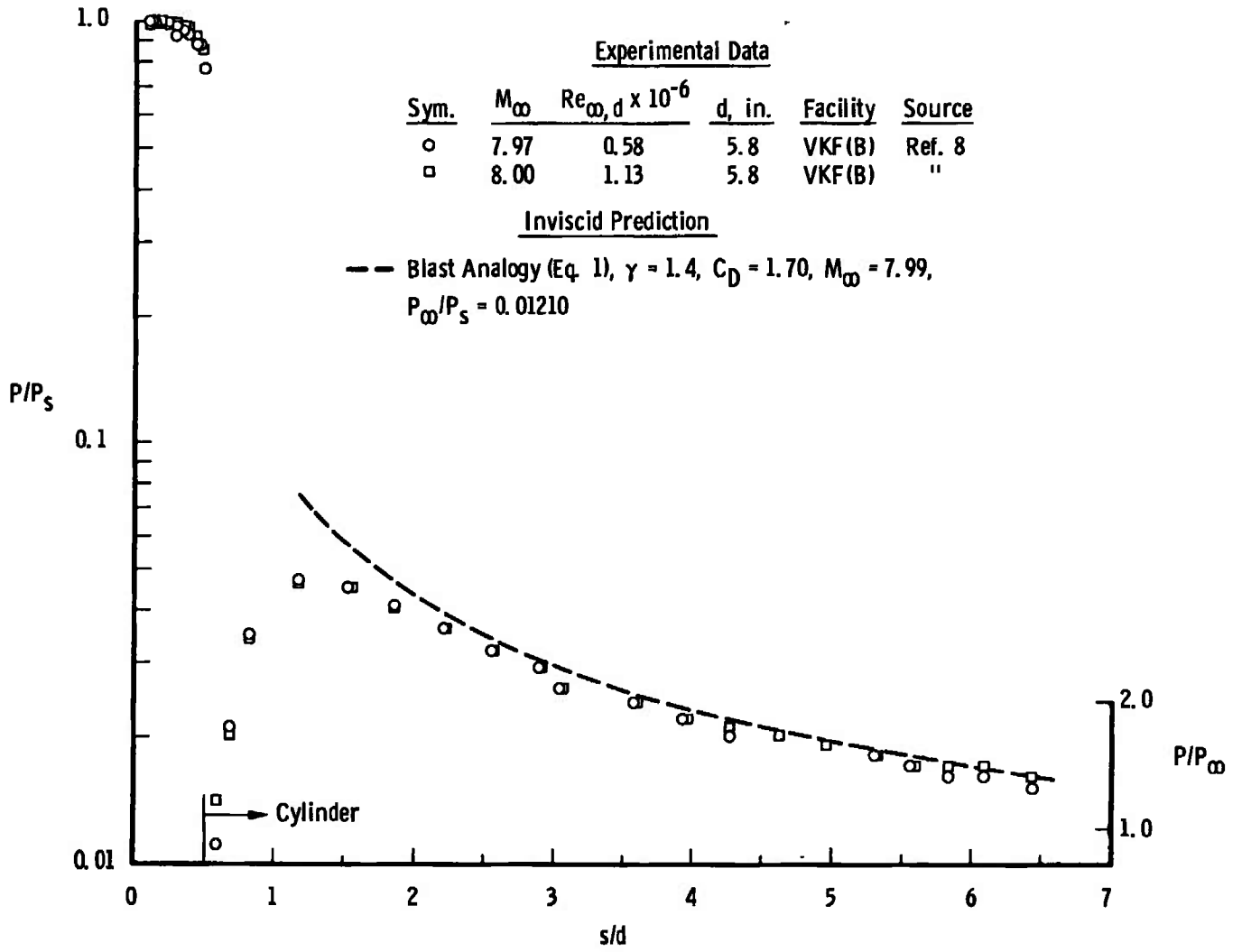

Fig. 7 Experimental and Theoretical Pressure Distributions on a Flat-Face Cylinder at Mach Number 8

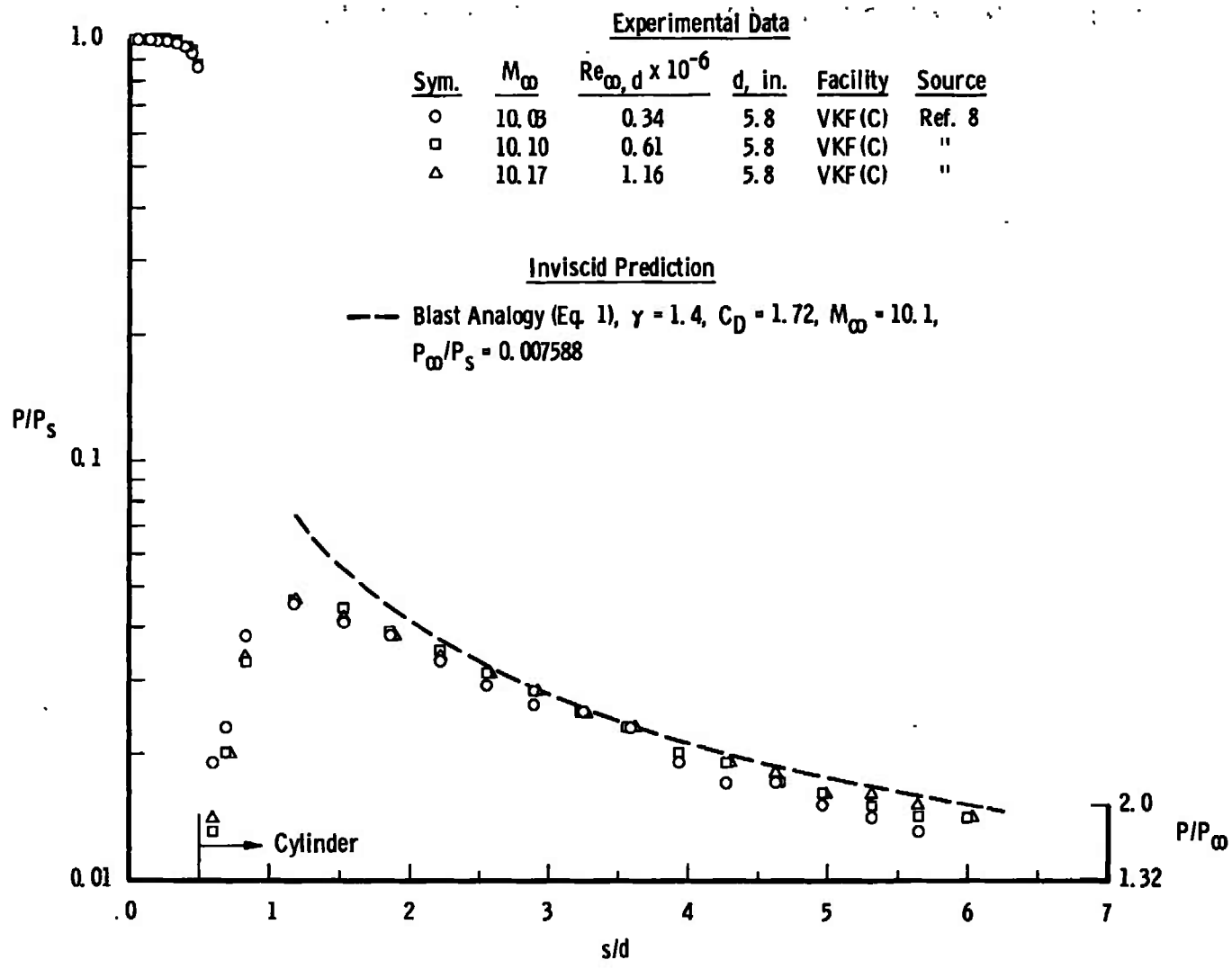

Fig. 8 Experimental and Theoretical Pressure Distributions on a Flat-Face Cylinder at Mach Number 10

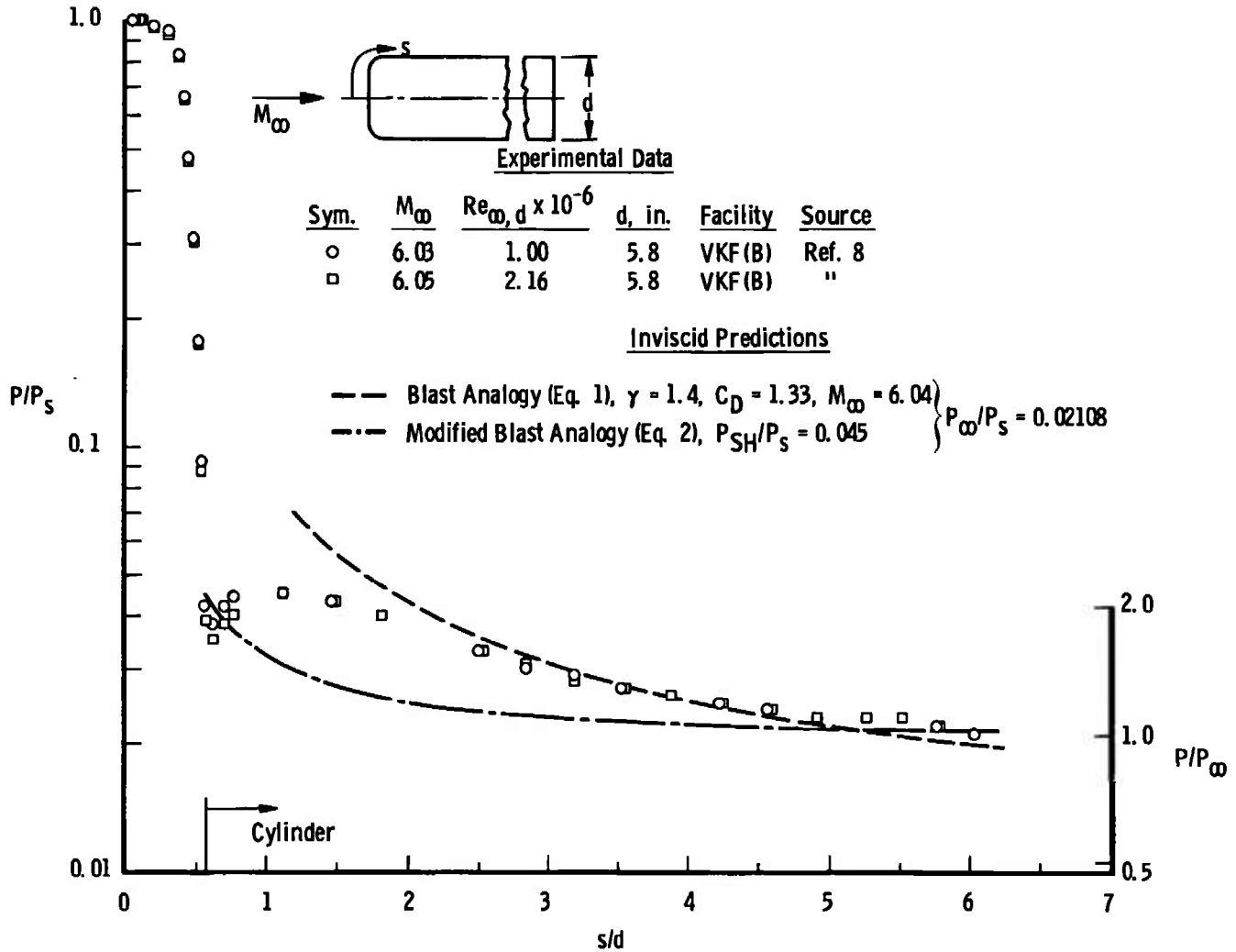

Fig. 9 Experimental and Theoretical Pressure Distributions on a Rounded-Shoulder Flat-Face Cylinder at Mach Number 6

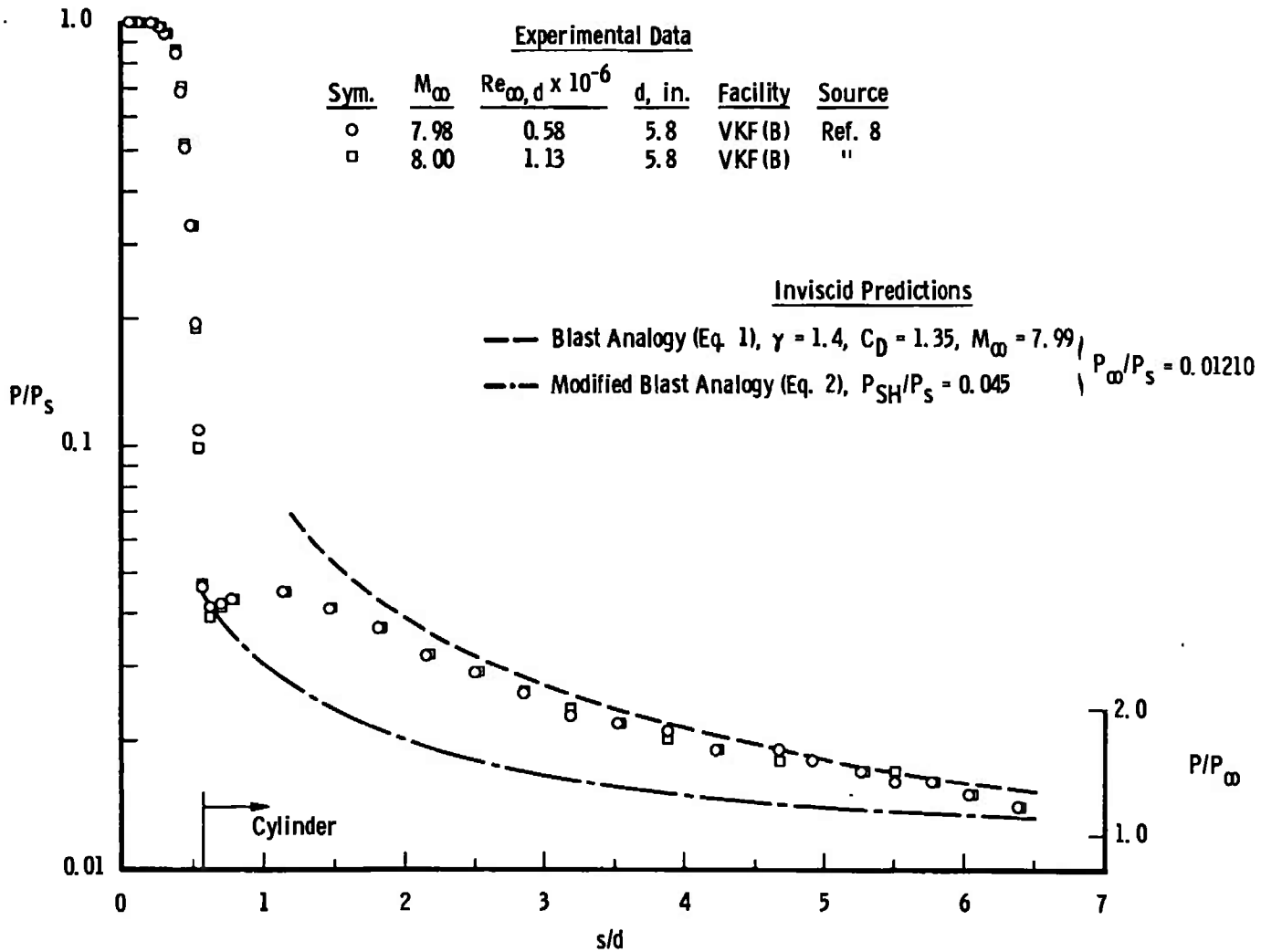

Fig. 10 Experimental and Theoretical Pressure Distributions on a Rounded-Shoulder Flat-Face Cylinder at Mach Number 8

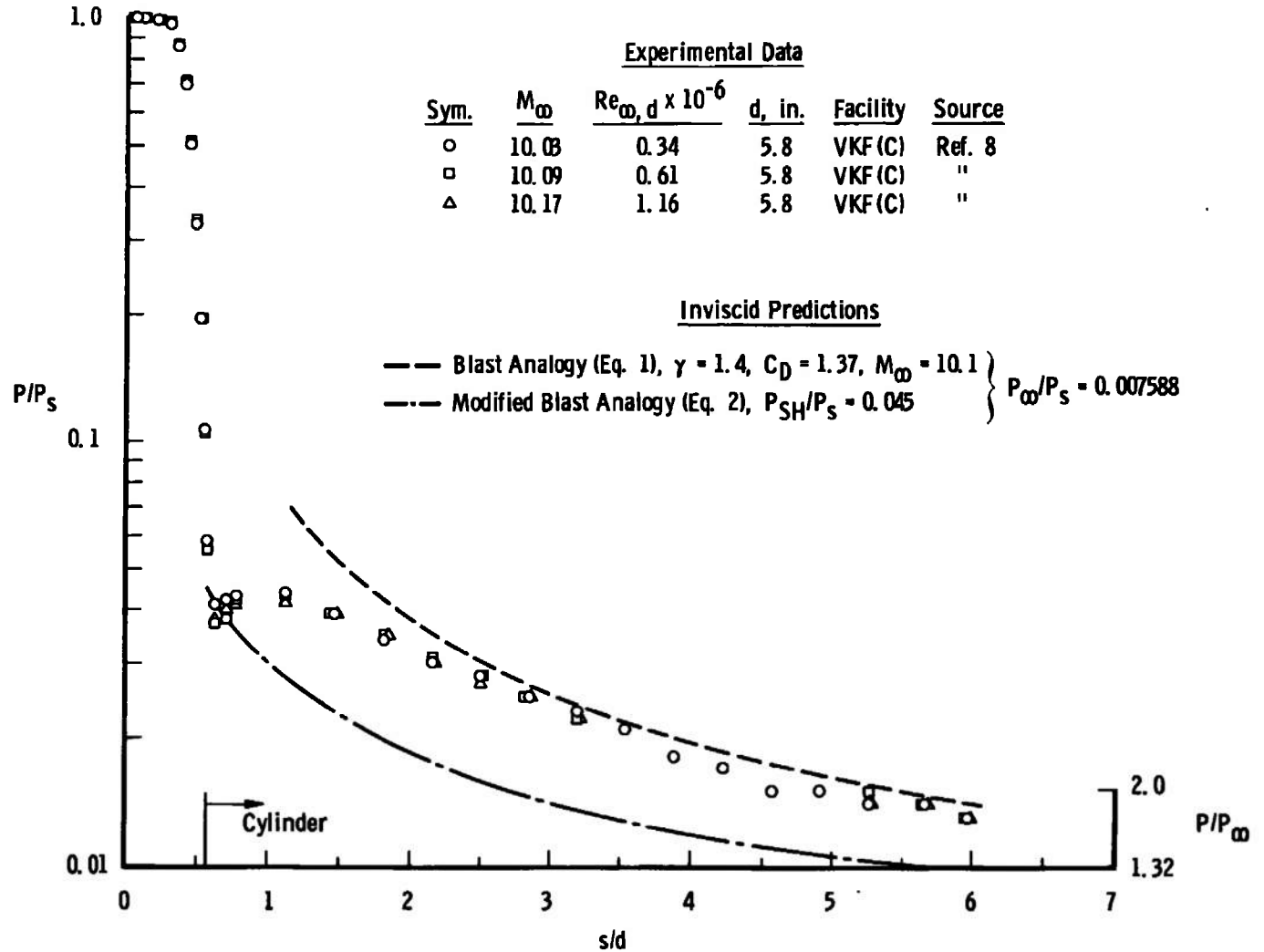

Fig. 11 Experimental and Theoretical Pressure Distributions on a Rounded-Shoulder Flat-Face Cylinder at Mach Number 10

increases immediately downstream of the tangent point. When applying the modified blast analogy, the selection of the shoulder pressure ratio (P_{SH}/P_s) again appears not to be the ideal pressure ratio to use for the best agreement with experiment.

The comparisons indicate that the characteristics solution results are in good agreement with hemisphere cylinder data; however, a proven method of obtaining starting conditions to generate a characteristics solution for the flat-face and rounded-shoulder flat-face cylinder is not known at the present time. Blast analogy results (Equation 1) compare favorably with all three models presented but only over a limited range ($s/d > 2.5$ and $P/P_\infty > 1.0$). The results of modified blast analogy (Equation 2), incorporating the pressure decay laws of Reference 20, indicate similar decay characteristics as the experimental data; however, extreme difficulty was encountered in selecting a shoulder pressure ratio that would predict the cylinder pressures.

In conclusion, a need has been shown for a readily solvable equation to predict the pressure distribution on blunt-nosed cylindrical afterbodies at hypersonic Mach numbers.

II. PROCEDURE FOR OBTAINING THE CORRELATING EQUATION

To simplify the procedure, the afterbody pressure data at each nominal Mach number at different Reynolds numbers have been averaged and are given in Figures 12 through 14. As previously mentioned, the high Reynolds number data presented in Figures 3 through 11, pages 17

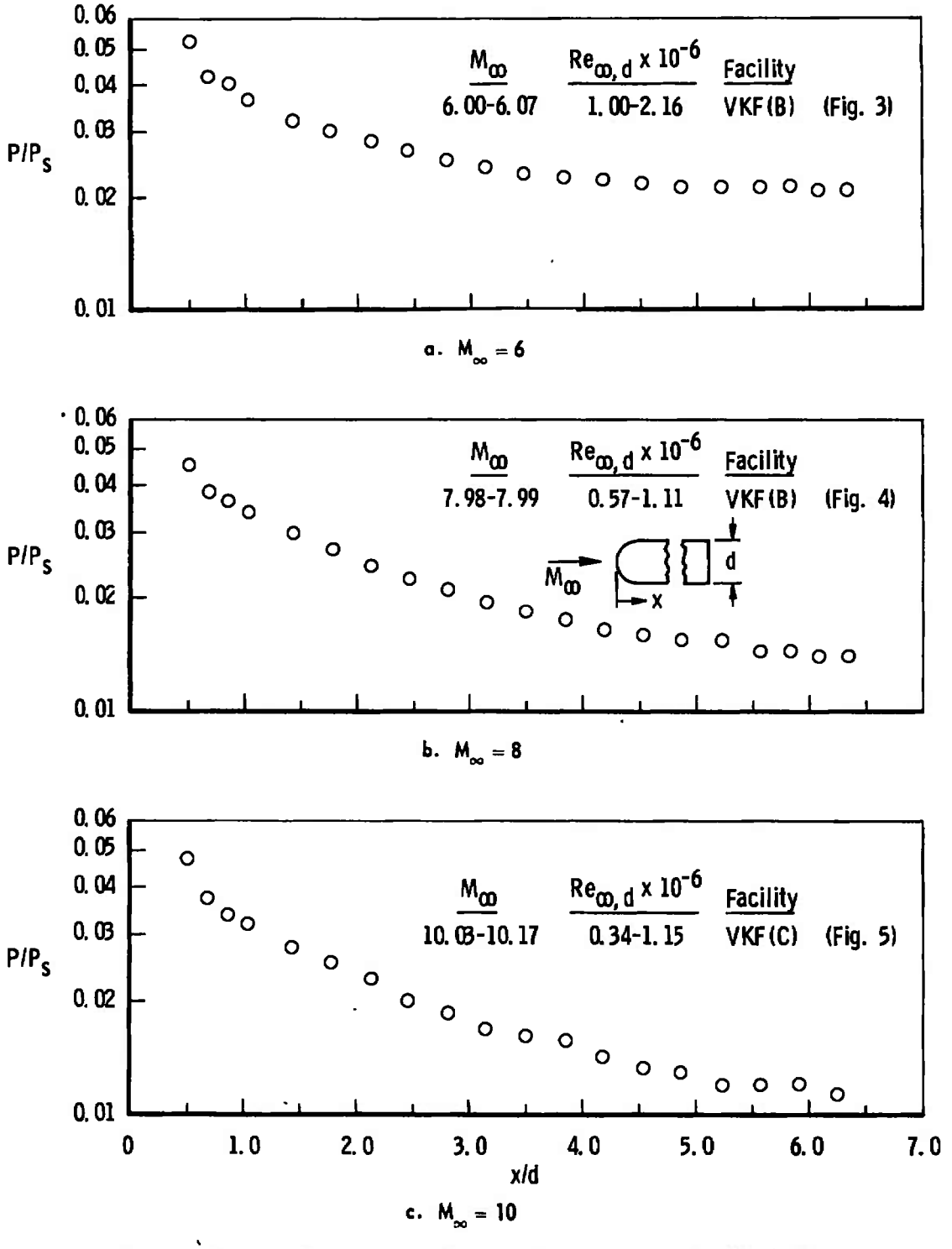

Fig. 12 Averaged Experimental Pressure Distribution on the Afterbody of a Hemisphere Cylinder at Mach Numbers 6, 8, and 10

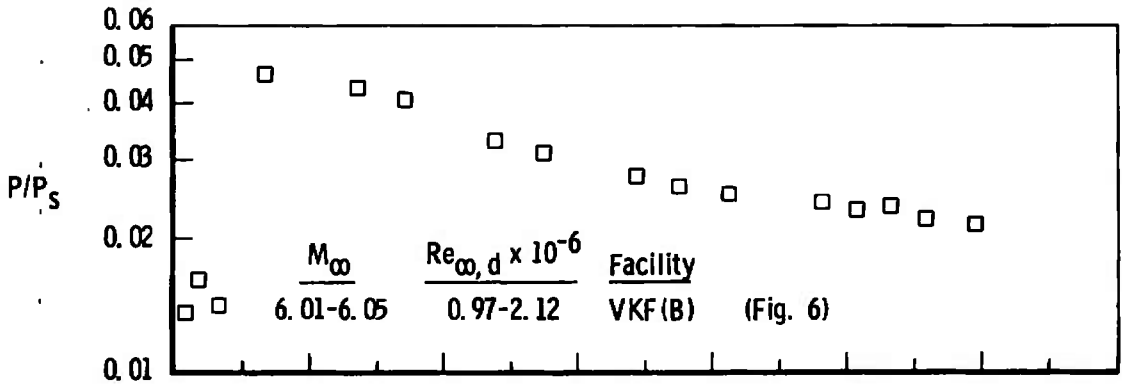

a. $M_\infty = 6$

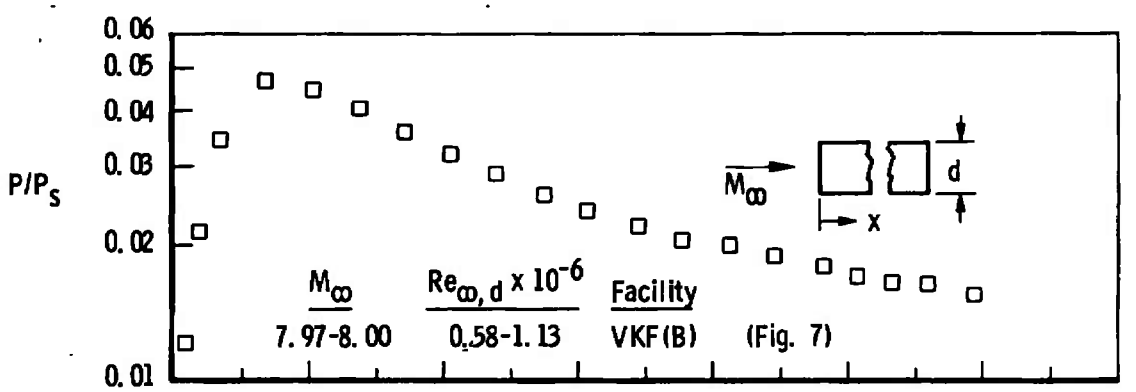

b. $M_\infty = 8$

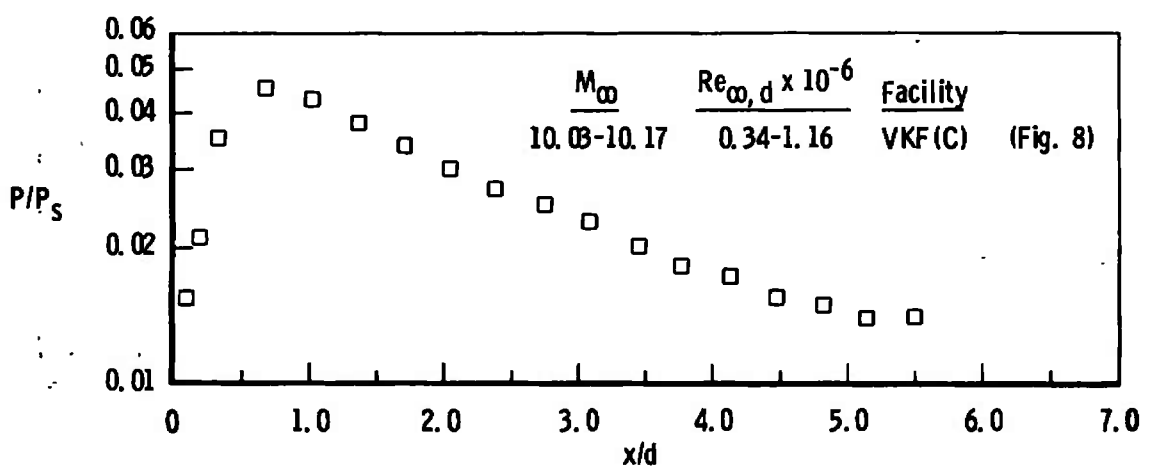

c. $M_\infty = 10$

Fig. 13 Averaged Experimental Pressure Distribution on the Afterbody of a Flat-Face Cylinder at Mach Numbers 6, 8, and 10

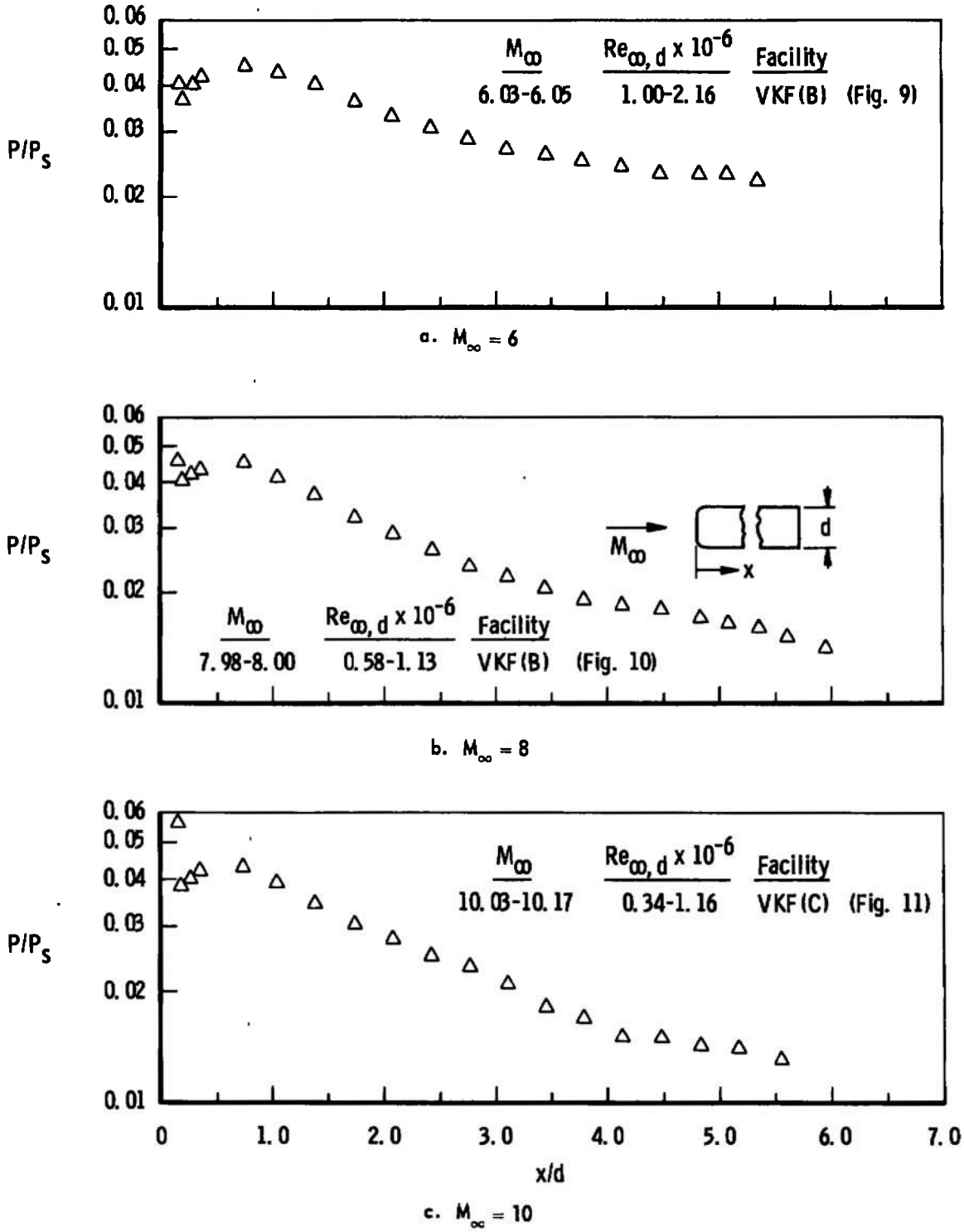

Fig. 14 Averaged Experimental Pressure Distribution on the Afterbody of a Rounded-Shoulder Flat-Face Cylinder at Mach Numbers 6, 8, and 10

through 26, show no significant decrease in pressure by increasing the Reynolds number; therefore, viscous effects are considered negligible. However, viscous effects are discernible in the overexpanded regions of the flat-face and rounded-shoulder flat-face cylinder. For obvious reasons, these overexpanded regions are not considered for correlation purposes.

For a constant Mach number over the approximate same Reynolds number range, the obvious differences in the three bodies considered are the nose geometry and nose pressure drag. By assuming that blunt nose shapes do not influence the afterbody pressure, the nose drag coefficient (C_D) should be the parameter to correlate the pressure distributions at each Mach number. From the work of various authors, an insight for correlating these afterbody pressures with nose drag is obtained. Casaccio (23) in 1958 noted that a shift or axial translation upstream of the nose would improve the agreement of a $M_\infty = 20$ hemisphere cylinder characteristics solution with blast analogy results. Vaglio-Laurin and Trella (24) suggested an upstream shift of one nose diameter from the nose apex for better agreement with blast analogy. The theoretical pressure data of Van Hise (14) and various experimental hemisphere cylinder data were correlated by Lukasiewicz (25) with Equation 1 by shifting the origin upstream one diameter for all nose shapes considered. Lukasiewicz's results were in good agreement with the Van Hise calculations but underpredicted the experimental pressure data. Lukasiewicz (25) also

demonstrated that the shift or displacement required to correlate shock shapes of blunt-nosed cylinders with blast analogy is a linear function of the drag coefficient only. Since the magnitude of such a shift cannot at present be determined theoretically, Kuehn (26) suggested the proper amount to shift the origin can be determined only by examining many cases. The present experimental data of three nose shapes and three Mach numbers afforded an opportunity to determine the axial shift required for correlating these data.

Since the drag coefficient of the flat-face cylinder may be considered as an upper limit, the flat-face cylinder is an obvious selection as the reference nose geometry for zero shift. At a constant Mach number, for example $M_\infty = 6$, the origin of the flat-face cylinder data (Figure 13a, page 29) is held stationary and the hemisphere cylinder data of Figure 12a, page 28, are translated along the same axial coordinate until the pressure distributions of the two bodies coincide. The same procedure is then followed for the rounded-shoulder flat-face cylinder. The translation required to match the pressure distribution for each case is then the axial shift ($\Delta x/d$) or origin displacement needed to correlate the cylinder data at $M_\infty = 6$. The same method is then used at $M_\infty = 8$ and 10.

The results of the above mentioned shifting procedure are given in Figures 15 through 17. Only values of $x/d \geq 0.5$ are shifted due to the overexpanded region of the flat-face and rounded-shoulder flat-face cylinder and since $x/d = 0.5$ represents the tangent point of the hemisphere cylinder. Each figure illustrates the shift

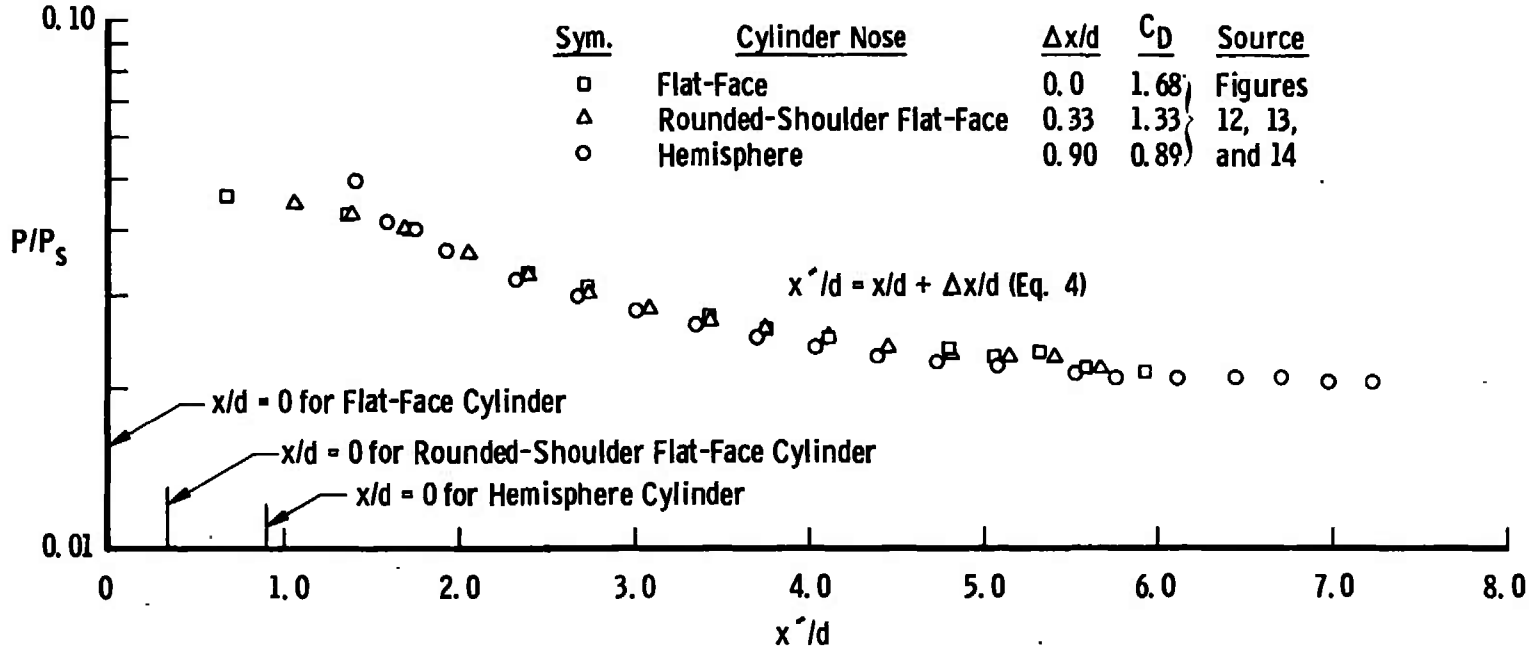

Fig. 15 Translated Afterbody Pressure Distributions at Mach Number 6

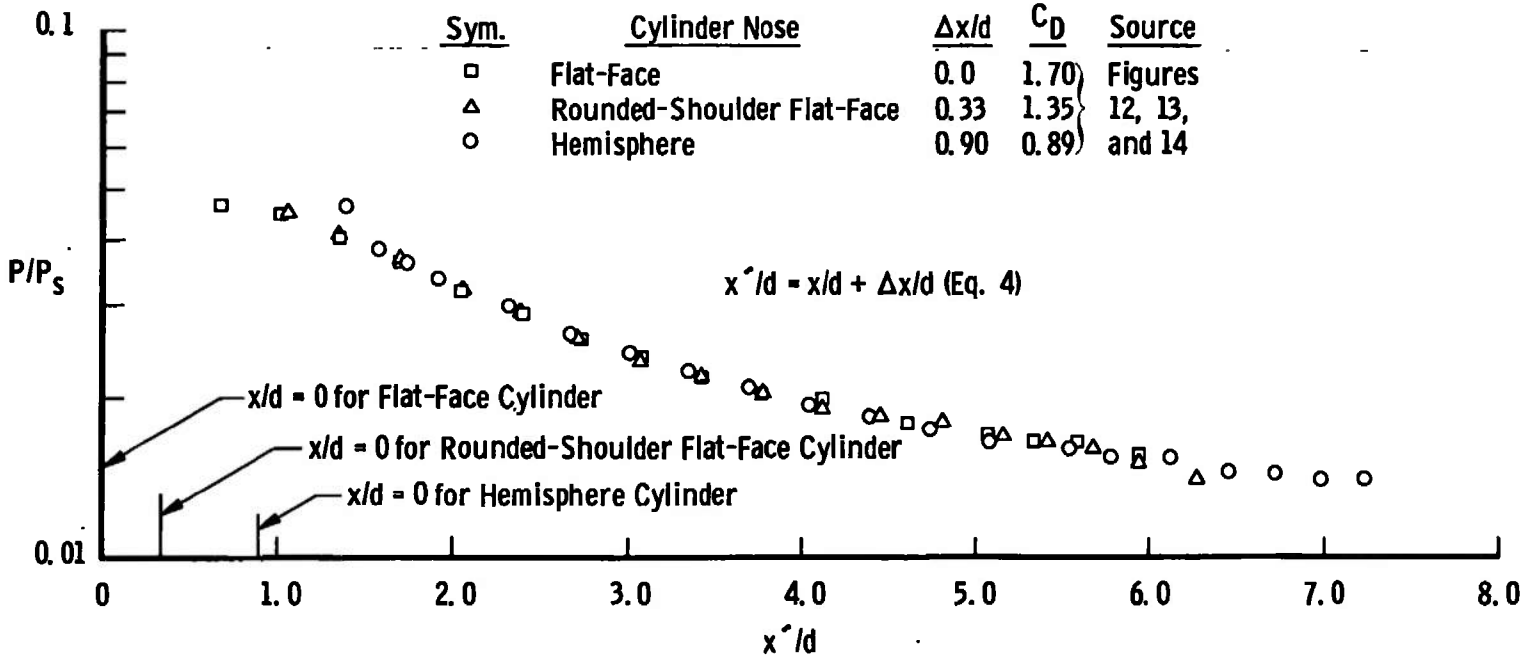

Fig. 16 Translated Afterbody Pressure Distributions at Mach Number 8

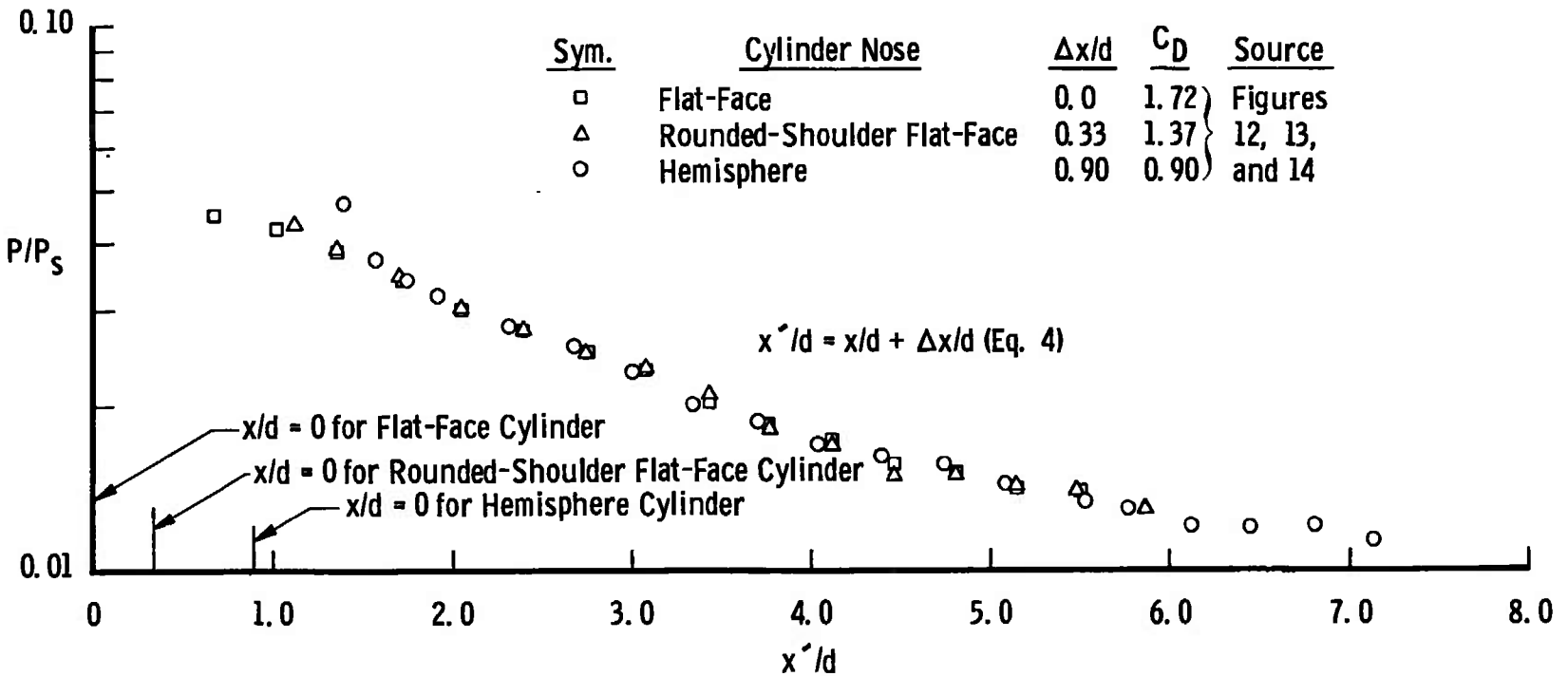

Fig. 17 Translated Afterbody Pressure Distributions at Mach Number 10

required for the three geometry configurations considered at M_∞ = 6, 8, and 10, respectively.

The translated parameter is then written as follows:

$$x'/d = x/d + \Delta x/d, \tag{4}$$

where x is measured along the model axis from the stagnation point and Δx is the upstream axial shift measured from the stagnation point. Since the nose drag is essentially constant for a particular nose shape for the M_∞ = 6, 8, and 10 data presented herein and the shift is assumed a function of the drag coefficient (C_D) only, the axial shift is assumed independent of Mach number for Mach numbers equal to and greater than 6. Cox and Crabtree (27) present sphere and cone cylinder drag data that are independent of Mach number for $M_\infty \geq 5.0$. Mach number independence on blunt nose bodies has been discussed by several authors (see Reference 27, for example) and is referred to as the "independence principle".

As mentioned above, the nondimensionalized axial shift ($\Delta x/d$) is assumed to be a function of the nose drag coefficient. The axial shift results are given as a function of the drag coefficient in Figure 18. An approximate representation is

$$\Delta x/d = - 1.08\ C_D + 1.836. \tag{5}$$

As pointed out above the nose drag coefficient for the bodies considered herein is considered to be independent of Mach number, consequently, the drag values in Figure 18 are average values for each

Sym.	Cylinder Nose	Δx/d	C_D*
□	Flat-Face	0.0	1.70
△	Rounded-Shoulder Flat-Face	0.33	1.35
○	Hemisphere	0.90	0.89

*C_D Averaged for Mach Numbers 6, 8, and 10

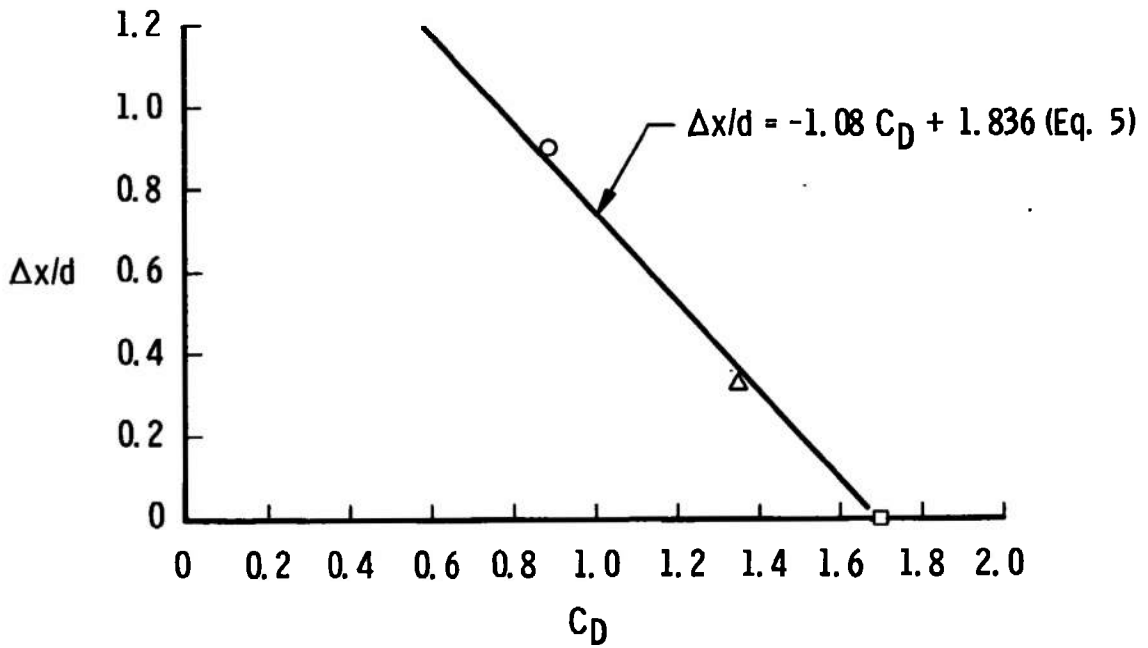

Fig. 18 Axial Shift versus Nose Drag Coefficient at Mach Numbers 6, 8, and 10

cylinder nose.

With the different body pressures in good agreement at each Mach number (Figures 15 through 17, pages 33 through 35) and the axial shift equation determined (Equation 5), the next task is arriving at a Mach number dependence relation to completely correlate the data. Figure 19 illustrates the good correlation obtained by plotting the translated afterbody pressure data of Figures 15 through 17 on log-log coordinates. Pressure data are presented only for $P/P_\infty \geq 1.0$. A straight line correlates the data with good accuracy at all three Mach numbers. The pressure of the flat-face and rounded-shoulder flat-face cylinder apparently remains overexpanded until x'/d is approximately equal to 1.37. The hemisphere cylinder data at x'/d = 1.4 (the highly sensitive tangent point) are approximately 12 per cent high but in excellent agreement immediately downstream. Note in Figure 19a the apparent increase in the pressure as x'/d = 5 is approached ($P/P_\infty = 1.0$ when $P/P_S = 0.0214$ at $M_\infty = 6$). As mentioned above, pressure data are not presented here for P/P_∞ less than 1.0 since the decay rate of the pressure distribution changes and the correlating equation becomes more involved. The character of the pressure decay will be discussed in more detail later in this chapter.

The pressure distribution is then correlated by an equation of the form

$$P/P_S = K(x'/d)^m \quad . \tag{6}$$

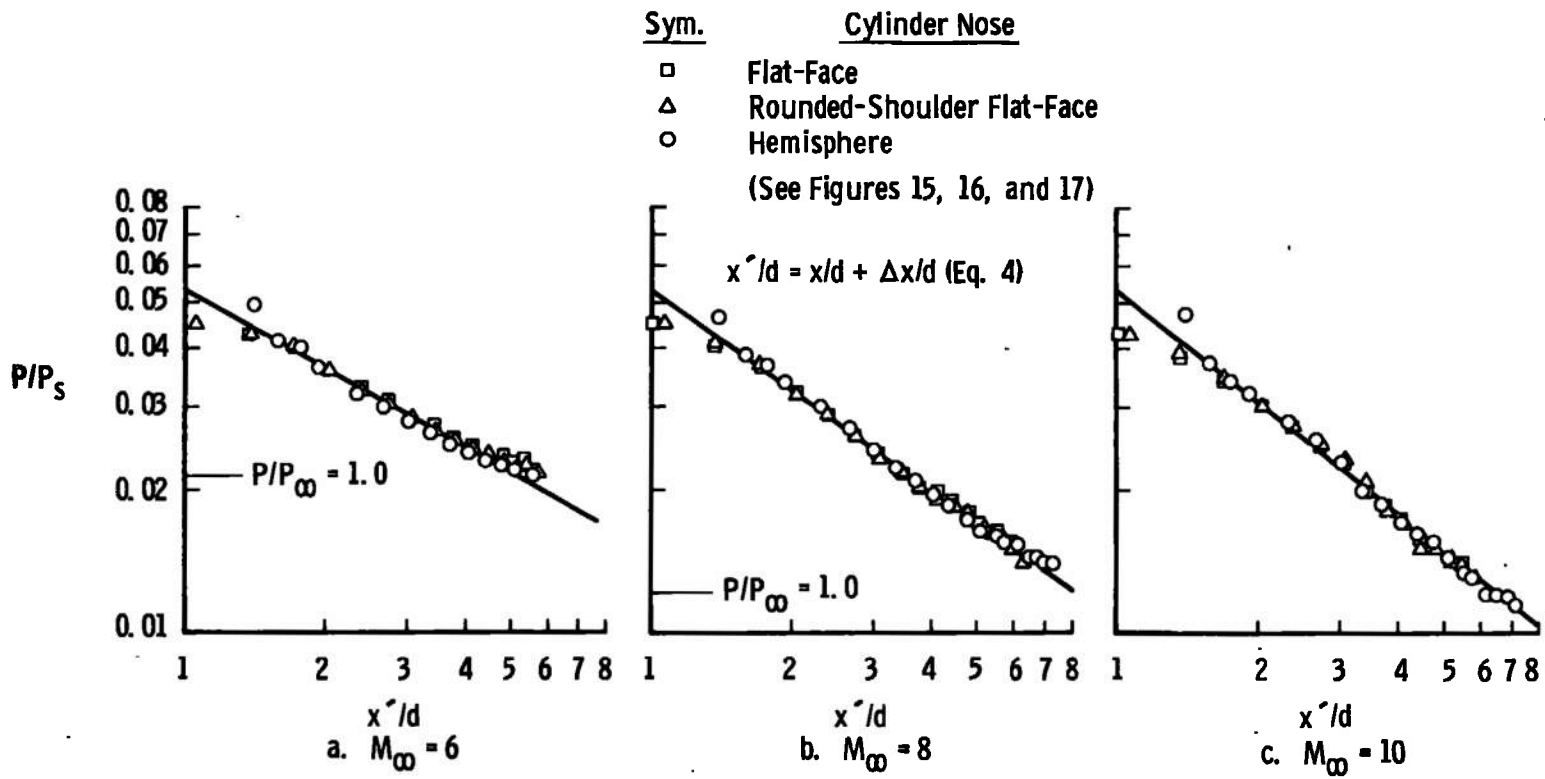

Fig. 19 Correlation of Translated Afterbody Pressure Distributions at Mach Numbers 6, 8, and 10

At x'/d of 1.0, the value of K equals 0.053 at M_∞ = 6, 8, and 10. The fact that K has the same value for all three Mach numbers is felt to be fortuitous and not necessarily indicative of the K value at other Mach numbers. The parameter (K) will be discussed further in this chapter. By combining Equations 4 and 5 with Equation 6, the resulting expression may be written

$$P/P_s = 0.053\ [x/d - 1.08\ C_D + 1.836]^m. \tag{7}$$

The exponent (m) of Equation 7 is shown versus $1/M_\infty$ in Figure 20. The resulting linear relation obtained for determining the exponent (m) is as follows:

$$m = 3.51\ (1/M_\infty) - 1.139. \tag{8}$$

Substituting Equation 8 into Equation 7 the final correlating equation is

$$P/P_s = 0.053\ [x/d - 1.08\ C_D + 1.836]^{3.51\ (1/M_\infty)-1.139}. \tag{9}$$

III. COMPARISONS OF VARIOUS DATA WITH THE CORRELATING EQUATION

Comparisons of the correlating equation results with experimental and theoretical data are presented to establish the agreement with other data and to investigate the limits of applicability of the correlation. A simplifying parameter, $\overline{R}$, is defined as

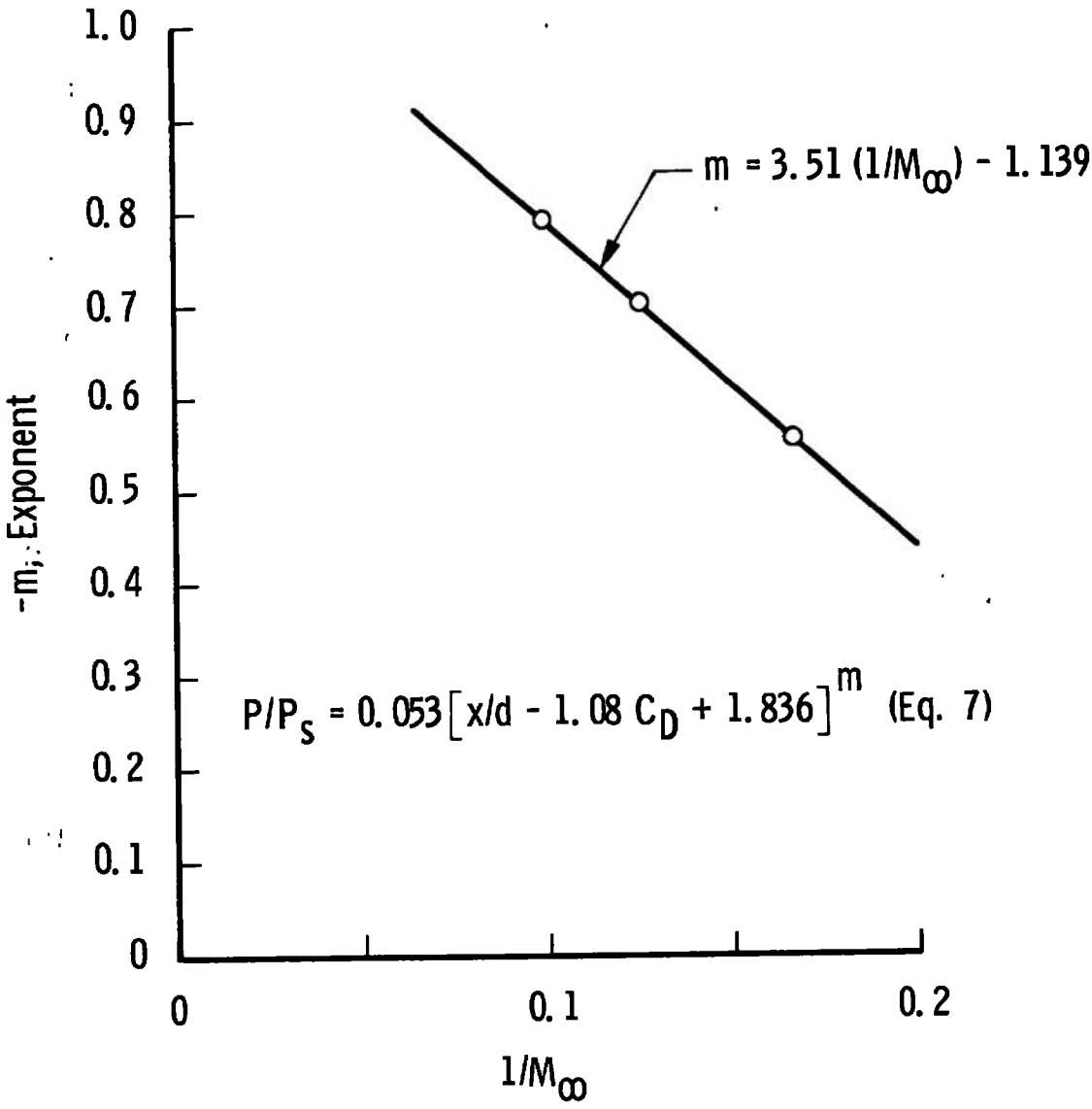

Fig. 20 Exponent of the Correlated Equation at Mach Numbers 6, 8, and 10

$$\bar{R} = [x/d - 1.08\ C_D + 1.836]^{3.51(1/M_\infty)-1.139}, \qquad (10)$$

so that Equation 9 may now be written as

$$P/P_S = 0.053\ \bar{R}. \qquad (11)$$

The final correlating equation (Equation 11) is compared with the experimental correlating data in Figure 21. Once the pressure continues to decrease aft of the cylinder junction ($1/\bar{R} \gtrsim 1.3$), an excellent correlation is evident. The increase in the pressure at $1/\bar{R} \gtrsim 2.5$ is the $M_\infty = 6$ data that is approaching $P/P_\infty = 1.0$ and should not be expected to correlate. Excluding the far downstream $M_\infty = 6$ data ($2.3 \leq 1/\bar{R} \leq 2.7$), 95 per cent of the data are within ±5 per cent for the $1/\bar{R}$ range from 1.3 to 4.8.

Additional data from various aerodynamic testing facilities are compared with Equation 11 in Figure 22, page 44 (note the x/d range presented). Unfortunately, in this case, the majority of available experimental models have a hemisphere nose resulting in a limited range of drag coefficients for comparison. However, many interesting observations are still presented. For the moment, excluding the sphere-cone-arc cylinder data ($C_D = 0.5$) of Gray (28) and Edenfield (29), an excellent correlation is obtained with the hemisphere and cut-sphere cylinder data for $1.3 \leq 1/\bar{R} \leq 6.0$. The $1/\bar{R}$ value of 1.3 as previously discussed is again taken as a minimum limit. Although The $M_\infty = 4$ data of Baer (30) is for $1/\bar{R}$ less than 1.3, the disagreement with the correlation is felt to be because of the parameter (K).

Sym.	Cylinder Nose	M_∞	C_D	$\Delta x/d$	x/d Range	Facility	Source
○	Hemisphere	6.03	0.89	0.88	0.5 -4.5	VKF(B)	Ref. 8 and Fig. 12
◐	Hemisphere	7.99	0.89	0.88	0.5 -6.3	VKF(B)	"
◑	Hemisphere	10.10	0.90	0.87	0.5 -6.3	VKF(C)	"
□	Flat-Face	6.03	1.68	0.02	1.4 -5.9	VKF(B)	Fig. 13
■	Flat-Face	7.99	1.70	0.00	1.0 -5.9	VKF(B)	"
◨	Flat-Face	10.10	1.72	-0.02	1.0 -5.5	VKF(C)	"
△	Rounded-Shoulder Flat-Face	6.04	1.33	0.40	0.73-5.3	VKF(B)	Fig. 14
▲	Rounded-Shoulder Flat-Face	7.99	1.35	0.38	0.73-5.9	VKF(B)	"
▲	Rounded-Shoulder Flat-Face	10.10	1.37	0.36	0.73-5.5	VKF(C)	"

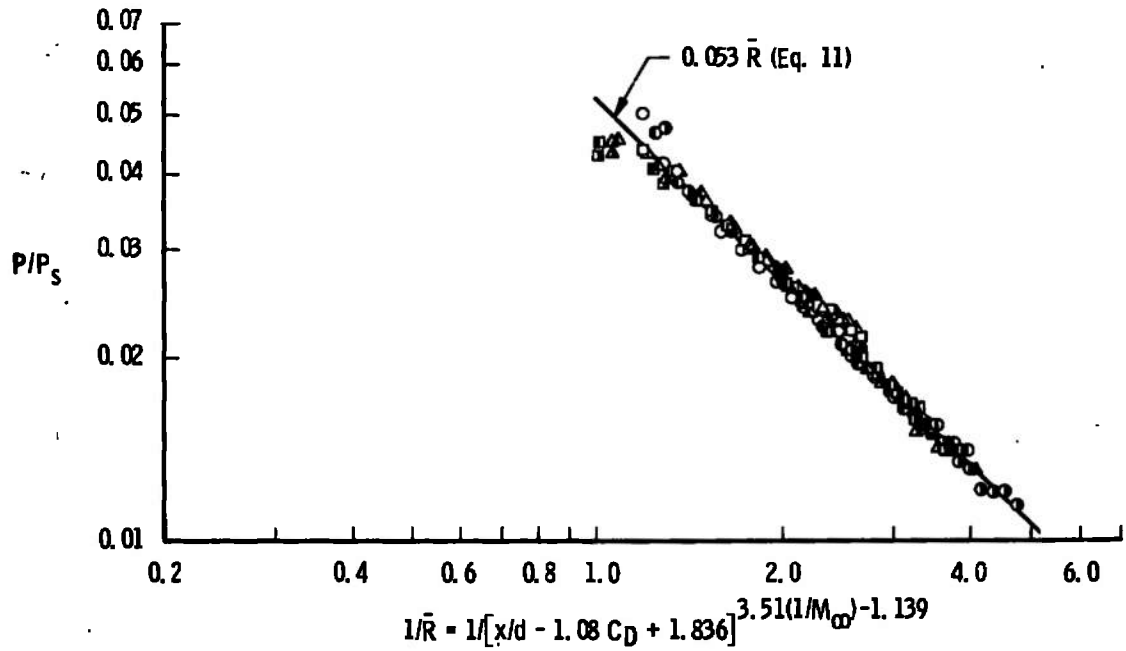

Fig. 21 Correlation of the Experimental Data

Sym.	M_∞	Diam., in.	$Re_{\infty,d} \times 10^{-6}$	C_D	$\Delta x/d$	x/d Range	Source
D	8.08	4.0	0.5 -1.0	0.5	1.29	2.0-5.6	Gray
D	19.3	4.0	≈0.076	0.5	1.29	1.8-4.4	Ref. 28
D	17.9	6.27	≈0.38	0.5	1.29	2.0-8.5	Edenfield, Ref. 29
o	4.03	5.8	2.55	0.87	0.89	0.5-1.4	Baer
□	5.06	↓	2.96	0.88	0.89	0.5-2.5	Ref. 30
◇	6.02	↓	1.91	0.89	0.87	0.5-5.2	↓
◁	8.1	↓	1.28	0.90	0.86	0.5-5.9	↓
o	6.83	---	0.27-0.36	0.91	0.84	1.0-6.0	Bertram & Henderson
o	9.6	---	0.06-0.11	0.91	0.84	0.5-9.0	Ref. 31
☆	6.87	3.0	1.0	0.91	0.84	0.5-3.3	Crawford & McCauley Ref. 32
▽	7.7	0.75	0.13	0.914	0.84	0.5-7.9	Lees & Kubota Ref. 3
o	≈19.2	4.0	0.032	0.91	0.84	0.5-7.5	Matthews
▽	≈18.9	1.0	0.013	0.91	0.84	0.8-4.7	Ref. 8
△	7.92	5.8	0.47	1.51	0.2	1.0-5.9	Matthews
◁	8.01	5.8	1.74	1.51	0.2	1.0-5.9	Ref. 33

All $C_D \approx 0.9$ data are hemisphere cylinders.

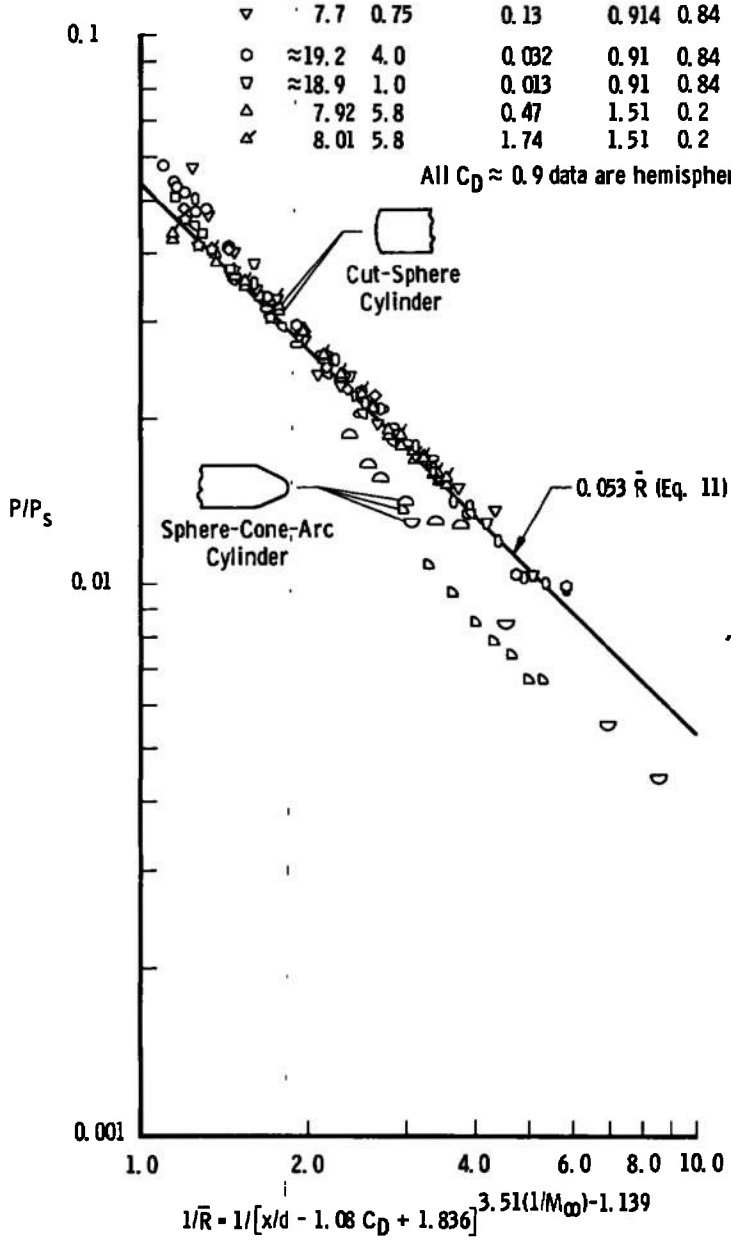

Fig. 22 Correlation of Additional Experimental Data

As previously discussed, page 40, a constant value of K (K = 0.053) was obtained from the experimental data at Mach numbers 6, 8, and 10. Then for a Mach number less than 5, these data indicate that K should be larger. This conclusion is verified later with characteristics solutions at various Mach numbers. Therefore, for $5 \leq M_\infty \leq 19.2$, $0.89 \leq C_D \leq 1.51$, and $1.3 \leq 1/\bar{R} \leq 6.0$, 95 per cent of these additional data are within ±10 per cent of the correlating equation. The majority of these data are presented either from the cylinder junction or immediately downstream. The low drag data (C_D = 0.5) of the sphere-cone-arc cylinder are presented to illustrate an apparent deficiency of the correlation. The axial shift ($\Delta x/d$) being a linear function of the drag apparently is not valid for a nose drag coefficient of 0.5. The axial shift relation (Equation 5) predicts a shift of 1.29 for the C_D = 0.5 results which is not satisfactory for correlating the pressure data. An axial shift, $\Delta x/d$, of approximately 3.0 is required for a good correlation with these data. The disagreement of Equation 11 with low drag ($C_D \approx 0.5$) pressure data will be further illustrated with characteristics solutions.

To further investigate the limits of the correlating parameter ($1/\bar{R}$), results from characteristics solutions, predominately for hemisphere cylinders, are presented in Figure 23. Since the correlation is limited to P/P_∞ greater than 1.0, free-stream Mach numbers from 4 to 100 are presented to extend the value of $1/\bar{R}$ and to investigate the validity of using a linear function of m (Equation

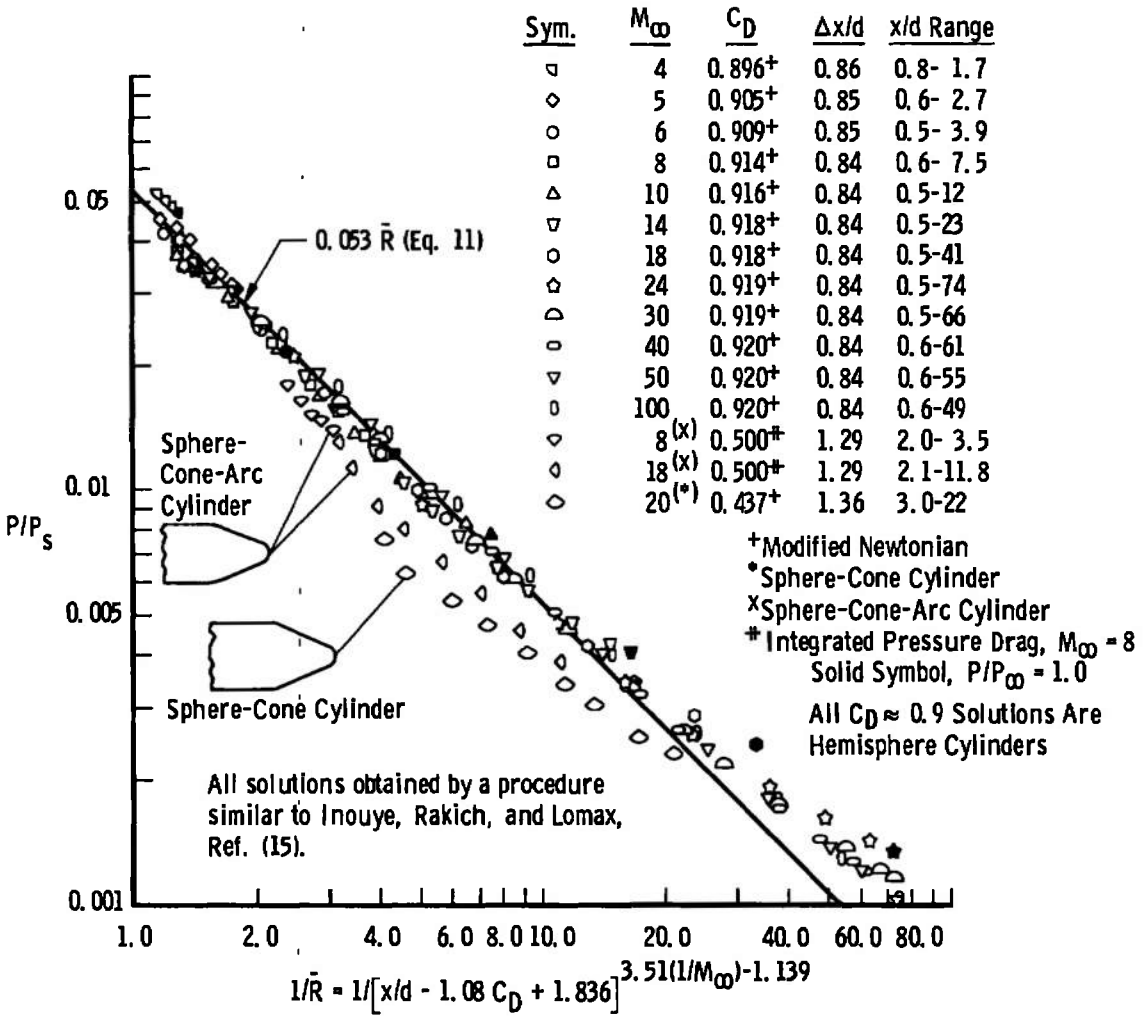

Fig. 23 Correlation of Method of Characteristics Solutions for Spherically Blunt Cylinders at Mach Numbers 4 to 100

8). Ninety-five per cent of the hemisphere cylinder solutions are within ±10 per cent of Equation 10 for $1.3 \leq 1/\bar{R} \leq 15.0$ and free-stream Mach numbers from 5 to 100. From these data it is concluded that the poor correlation for $1/\bar{R}$ greater than 15 is because the M_∞ = 14, 18, and 24 data extend to $P/P_\infty = 1.0$, and the decay characteristics for Mach numbers greater than 14 have changed. This will be discussed further with Figure 24. Note, the values of $P/P_\infty = 1.0$ are indicated with a solid symbol for each appropriate Mach number. These solutions for $1/\bar{R}$ greater than 15 indicate the decay of the pressure distribution no longer varies linearly with x'/d for $M_\infty > 14$ as depicted in Figure 19, page 39. A linear variation is evident, however, for all Mach numbers over a limited range ($1.3 \leq 1/\bar{R} \leq 15.0$).

Also presented in Figure 23 are the results for three low drag bodies to substantiate the findings of the previously mentioned low drag experimental data of Figure 22, page 44. The M_∞ = 8 and 18 ($C_D = 0.5$) method of characteristics solutions are for the experimental data of the sphere-cone-arc cylinder presented in Figure 22. Again, a total axial shift, $\Delta x/d$, of approximately 3.0 is required for the $C_D = 0.5$ solutions to agree with Equation 11. Also included is a calculation for a sphere-cone cylinder ($C_D = 0.437$) at Mach number 20 showing that the lower drag body requires an axial shift even greater than 3.0 for good agreement.

To further illustrate the previously mentioned difficulty of extending the range of the correlating parameter ($1/\bar{R}$), characteristics

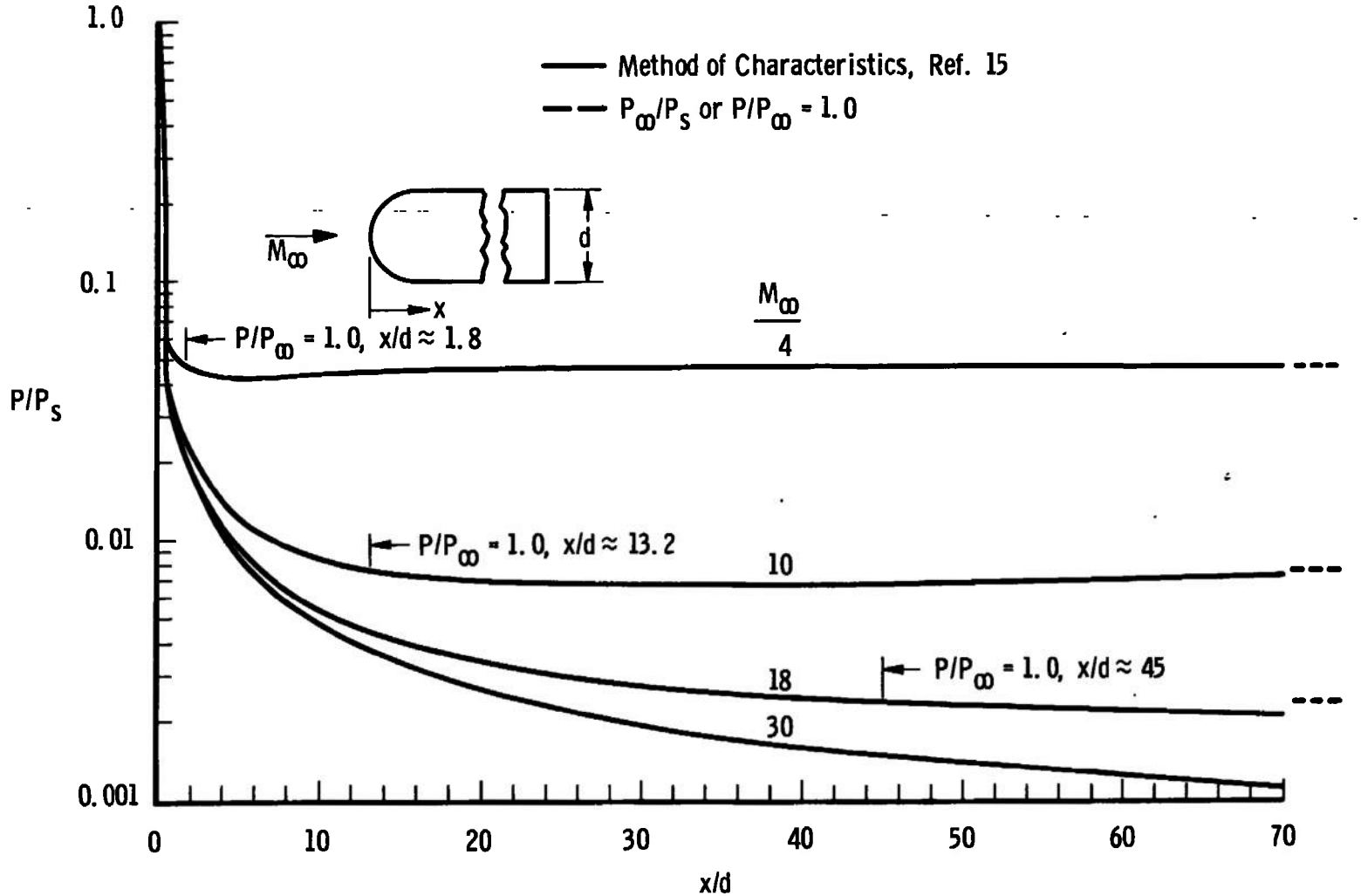

Fig. 24 Characteristics Solutions for Hemisphere Cylinders at Mach Numbers 4, 10, 18, and 30

solutions at various Mach numbers are presented for hemisphere cylinders in Figure 24. First, note how the cylinder length (x/d) for $P/P_\infty \geq 1.0$ varies with Mach number. The lower correlating pressure limit ($P/P_\infty = 1.0$) is obtained at $M_\infty = 4.0$ when $x/d \approx 1.8$ and at $M_\infty = 18$ when $x/d \approx 45$. One can observe from the solutions presented that the decay characteristics are different at the higher Mach numbers for x/d values greater than approximately 12. Since a larger x/d range is available at higher Mach numbers, the pressure gradient is more apt to change.

Also note as P_∞ is approached, the pressure gradient rapidly decreases and the pressure subsequently overexpands and recompresses. This is the reason no attempt is made to correlate pressures less than P_∞.

Since m was determined from experimental data for $x/d < 7.0$ at Mach numbers 6, 8, and 10, data beyond these limits help to determine the validity of the expression for m. The equation derived for the exponent (m), Equation 8, was shown to be valid in the range of $1.3 \leq 1/\bar{R} \leq 15$ for any Mach number in the range from 5 to 100.

The study of two bodies of equal nose drag but different nose shapes has received the attention of many workers. Mueller, Close, and Henderson (34) modified a hemispherical nose with a 90 degree conical tip so that the nose drag coefficient of the two models remained essentially constant. From this work it was found that the afterbody pressure distribution was essentially invariant with respect

to the two nose shapes. Additional studies by Witcofski and Henderson (35) found that for two models with the same nose drag coefficients ($0.2 \leq C_D \leq 1.2$) but different nose shapes, the pressure distribution was a function of nose drag only and independent of nose shape for $x/d \gtrsim 2.0$. The characteristics solutions of Van Hise (14) for a group of pointed-nosed cylinders over a wide range of Mach numbers and nose drag coefficients are presented in Figure 25. These results are included to study nose shape independence, and to compare the results with the correlation, Equation 11.

First, note that there are two pointed-nosed cylinders with the same nose drag as the cylinders previously used for correlating, namely, the hemisphere ($C_D = 0.87$) and rounded-shoulder flat-face ($C_D = 1.37$) cylinder. The pointed hemispherical nose ($C_D = 0.87$) agrees with the correlating equation at all Mach numbers presented. The pressure data of the conical nose ($C_D = 1.37$) agree well with the correlating equation at $M_\infty = 10$ but are 15 and 20 per cent high for $M_\infty = 20$ and 40, respectively. Again this is for a range of $1.3 \leq 1/\bar{R} \leq 15.0$. The pressure data of the low drag ogival nose ($C_D = 0.47$) indicate that a larger axial shift ($\Delta x/d \approx 2.5$) is required just as the previously mentioned low drag data.

These characteristics solutions of Van Hise (14) exhibit more scatter than the previous characteristics solutions of the hemisphere cylinder but represent a larger drag coefficient range ($0.47 \leq C_D \leq 1.37$). An overexpansion of the pressure distribution diminishes at

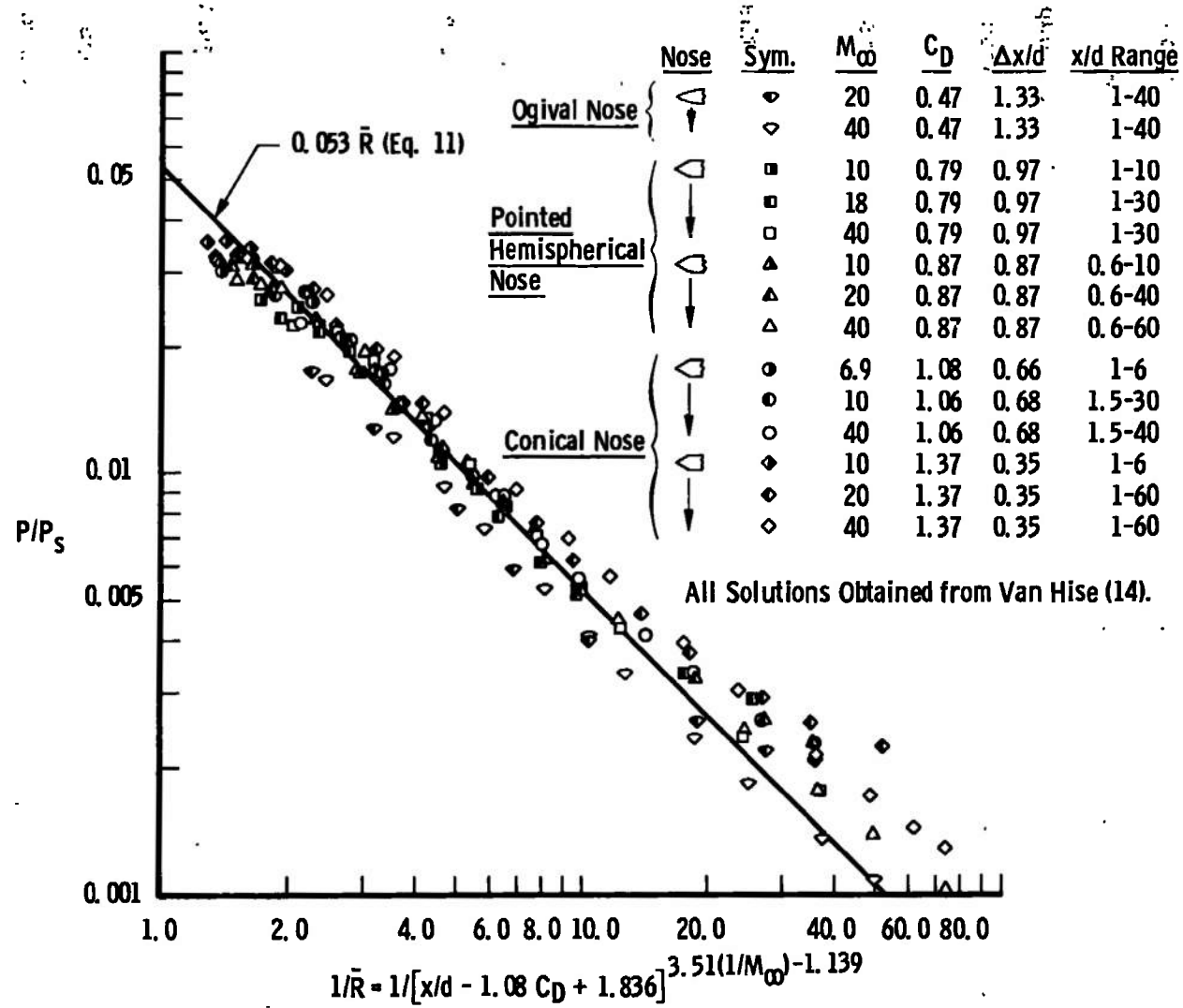

Fig. 25 Correlation of Characteristics Solutions for Various Pointed-Nosed Cylinders at Mach Numbers 6.9 to 40

$1/\bar{R} \gtrsim 2.0$ where 95 per cent of the data is observed to be within ±10 per cent of the correlating equation for $2.0 \leq 1/\bar{R} \leq 15.0$, $0.79 \leq C_D \leq 1.37$, and $6.9 \leq M_\infty \leq 40$ except the $M_\infty = 20$ and 40 data for the $C_D = 1.37$ solutions. The reasons of disagreement beyond $1/\bar{R} > 15.0$ as previously discussed with the characteristics solutions of Figure 23, page 46, are still considered valid for these solutions.

CHAPTER VI
CONCLUDING REMARKS

Afterbody pressure distributions over hemisphere, flat-face, and rounded-shoulder flat-face cylinders have been correlated at Mach numbers of 6, 8, and 10 for $0.34 \leq Re_{\infty,d} \times 10^{-6} \leq 2.16$. The final correlating equation was compared with additional experimental data and results of characteristics solutions over a wide range of Mach numbers and nose drag coefficients. These comparisons provided a means of analyzing the correlation's validity and limitations. As a result of these comparisons and other considerations, the following conclusions are drawn:

1. An equation (Equation 11) was developed that predicted the afterbody pressure distribution within ±10 per cent for 95 per cent of all available experimental data presented on blunt-nosed cylinders (C_D = 0.89 - 1.72) for $5 \leq M_\infty \leq 19.2$ and $1.3 \leq 1/\bar{R} \leq 6.0$. These data were all correlated approximately from the nose-cylinder junction when appropriate.
2. For $C_D \gtrsim 0.5$, it was shown with experimental data and results of characteristics solutions for blunt and pointed noses that a larger axial shift ($\Delta x/d$) than predicted is required for good agreement. Therefore, the axial shift apparently was not a linear function of

the nose drag coefficient.

3. For $C_D \approx 0.9$, the hemisphere cylinder characteristics solutions presented indicate good agreement for all Mach numbers ($5 \leq M_\infty \leq 100$) for $1.3 \leq 1/\bar{R} \leq 15.0$. The disagreement for $1/\bar{R} > 15.0$ was attributed to the decay characteristics changing with x/d and the pressure approaching free-stream.

4. The pressure distribution of the pointed-nosed cylinders indicated geometry shape independence for the range of nose drag coefficients correlated successfully ($0.79 \leq C_D \leq 1.37$), although there was some disagreement with the correlating results for the high Mach number ($M \geq 20$) and high drag coefficient ($C_D = 1.37$) solutions. The solutions of Van Hise essentially agreed with the hemisphere cylinder results by the method of characteristics for the same Mach number and $1/\bar{R}$ range considered.

5. For blunt-nosed cylinders ($C_D = 0.89 - 1.72$), the correlating equation (Equation 11) is considered applicable over the experimental range of Mach number from 5.0 to 19.2 and the correlating parameter ($1/\bar{R}$) from 1.3 to 6.0. Although a good correlation is obtained with the method of characteristics solutions over an extended range of Mach number and $1/\bar{R}$, the applicability of the correlating equation beyond the experimental limits has not been demonstrated.

BIBLIOGRAPHY

BIBLIOGRAPHY

1. Van Dyke, Milton D. "The Supersonic Blunt Slender Body Problem - Review and Extension," Journal of the Aeronautical Sciences, 25:485-495, August, 1958.

2. Van Dyke, Milton D. "The Blunt Body Problem Revisited," Fundamental Phenomena in Hypersonic Flow. Ithaca, New York: Cornell University Press, 1966. Pp. 52-64.

3. Lees, Lester and Toshi Kubota. "Inviscid Hypersonic Flow Over Blunt-Nosed Slender Bodies," Journal of the Aeronautical Sciences, 24:195-202, March, 1957.

4. Gold, Ruby and Maurice Holt. "Calculation of Supersonic Flow Past a Flat-Head Cylinder by Belotserkovskii's Method," Air Force Office of Scientific Research TN-59-199, Providence, Rhode Island, March, 1959.

5. Vinokur, Marcel. "The Distribution of Velocity, Pressure, and Laminar Heat Transfer on Blunt Bodies in Hypersonic Flow," Lockheed Missiles and Space Company 894815, Aerophysics Technical Note 3, Sunnyvale, California, May, 1961.

6. Lukasiewicz, J. "Hypersonic Flow - Blast Analogy," Arnold Engineering Development Center TR-61-4, Arnold Air Force Station, Tennessee, June, 1961.

7. Love, E. S. "Prediction of Inviscid Induced Pressures from Round Leading Edge Blunting at Hypersonic Speeds," ARS Journal, 26:792-794, October, 1959.

8. Matthews, R. K. Private Communication. Arnold Engineering Development Center, Arnold Air Force Station, Tennessee, September, 1967.

9. Fitch, C. R. "Flow Quality Improvement at Mach 8 in the VKF 50-Inch Hypersonic Wind Tunnel B," Arnold Engineering Development Center TR-66-82, Arnold Air Force Station, Tennessee, May, 1966.

10. Sivells, James C. "Aerodynamic Design and Calibration of the VKF 50-Inch Hypersonic Wind Tunnels," Arnold Engineering Development Center TDR-62-230, Arnold Air Force Station, Tennessee, March, 1963.

11. Howard, C. M. and H. T. Wood, Jr. "Mechanical Design of the 50-Inch Mach 10-12 Tunnel," Arnold Engineering Development Center TDR-62-229, Arnold Air Force Station, Tennessee, April, 1963.

12. Ames Research Staff. "Equations, Tables, and Charts for Compressible Flow," National Advisory Committee for Aeronautics Report 1135, Washington, D. C., 1953.

13. Randall, R. E. "Thermodynamic Properties of Air: Tables and Graphs Derived from the Beattie-Bridgeman Equation of State Assuming Variable Specific Heats," Arnold Engineering Development Center TR-57-8, Arnold Air Force Station, Tennessee, August, 1957.

14. Van Hise, Vernon. "Analytic Study of Induced Pressure on Long Bodies of Revolution with Varying Nose Bluntness at Hypersonic Speed," National Aeronautics and Space Administration TR R-78, Washington, D. C., 1961.

15. Inouye, M., J. V. Rakich, and H. Lomax. "A Description of Numerical Methods and Computer Programs for Two-Dimensional and Axisymmetric Supersonic Flow Over Blunt-Nosed and Flared Bodies," National Aeronautics and Space Administration TN D-2970, Washington, D. C., August, 1965.

16. Taylor, G. I. "The Formation of a Blast Wave by a Very Intense Explosion," Proceedings of the Royal Society (A), 201 (No. 1065):159-186, March, 1950.

17. Lin, S. C. "Cylindrical Shock Waves Produced by Instantaneous Energy Release," Journal of Applied Physics, 25 (No. 1): 54-57, January, 1954.

18. Sakurai, A. "On the Propagation and Structure of the Blast Wave, I," Journal of the Physical Society of Japan, 9 (No. 2): 662, September-October, 1953.

19. Sakurai, A. "On the Propagation and Structure of a Blast Wave, II," Journal of the Physical Society of Japan, 9 (No. 2): 256, March-April, 1954.

20. Cheng, H. K. and A. J. Palone. "Inviscid Leading-Edge Effect in Hypersonic Flow," Journal of Aeronautical Sciences, 23 (No. 7):700-702, July, 1956.

21. Clark, E. L. Private Communication. Arnold Engineering Development Center, Arnold Air Force Station, Tennessee, December, 1966.

22. Vaglio-Laurin, Roberto and Antonio Ferri. "Theoretical Investigation of the Flow Field Around Blunt-Nosed Bodies in Supersonic Flight," Journal of the Aeronautical Sciences, 25:761-770, December, 1958.

23. Casaccio, A. "Theoretical Pressure Distribution on a Hemisphere-Cylinder Combination," Journal of the Aeronautical Sciences, 26 (No. 1):63-64, January, 1959.

24. Vaglio-Laurin, Roberto and Massimo Trella. "A Study of Flow Fields About Some Typical Blunt-Nosed Slender Bodies," Polytechnic Institute of Brooklyn Report No. 623, Brooklyn, New York, December, 1960.

25. Lukasiewicz, J. "Blast-Hypersonic Flow Analogy Theory and Application," ARS Journal, 32 (No. 9):1341-1346, September, 1962.

26. Kuehn, Donald M. "Experimental and Theoretical Pressures on Blunt Cylinders for Equilibrium and Nonequilibrium Air at Hypersonic Speeds," National Aeronautics and Space Administration TN D-1979, Washington, D. C., November, 1963.

27. Cox, R. N. and L. F. Crabtree. Elements of Hypersonic Aerodynamics, New York: Academic Press, 1965.

28. Gray, J. Don. "Summary Report on Aerodynamic Characteristics of Standard Models HB-1 and HB-2," Arnold Engineering Development Center TDR-64-137, Arnold Air Force Station, Tennessee, July, 1964.

29. Edenfield, E. E. Private Communication. Arnold Engineering Development Center, Arnold Air Force Station, Tennessee, December, 1967.

30. Baer, A. L. "Pressure Distributions on a Hemisphere Cylinder at Supersonic and Hypersonic Mach Numbers," Arnold Engineering Development Center TN-61-96, Arnold Air Force Station, Tennessee, August, 1961.

31. Bertram, M. H. and A. Henderson. "Recent Hypersonic Studies of Wings and Bodies," ARS Journal, 31:1129, August, 1961.

32. Crawford, Davis H. and William D. McCauley. "Investigation of the Laminar Aerodynamic Heat-Transfer Characteristics of a Hemisphere-Cylinder in the Langley 11-Inch Hypersonic Tunnel at a Mach Number of 6.8," National Advisory Committee for Aeronautics Report 1323, Washington, D. C., 1957.

33. Matthews, Richard K. Private Communication. Arnold Engineering Development Center, Arnold Air Force Station, Tennessee, December, 1967.

34. Mueller, James N., William H. Close, and Arthur Henderson, Jr. "An Investigation of Induced-Pressure Phenomena on Axially Symmetric, Flow-Aligned, Cylindrical Models Equipped with Different Nose Shapes at Free-Stream Mach Numbers from 15.6 to 21 in Helium," National Aeronautics and Space Administration TN D-373, Washington, D. C., May, 1960.

35. Witcofski, Robert D. and Arthur Henderson, Jr. "Induced Pressures on Cylindrical Rods with Various Nose Drags and Nose Shapes at Mach Numbers of 17 and 21," National Aeronautics and Space Administration TN D-1266, Washington, D. C., 1962.

Security Classification

DOCUMENT CONTROL DATA - R & D

(Security classification of title, body of abstract and indexing annotation must be entered when the overall report is classified)

1 ORIGINATING ACTIVITY (Corporate author)	2a. REPORT SECURITY CLASSIFICATION
Arnold Engineering Development Center ARO, Inc., Operating Contractor Arnold Air Force Station, Tennessee	UNCLASSIFIED
	2b. GROUP N/A

3 REPORT TITLE

AN EMPIRICAL CORRELATION OF PRESSURE ON BLUNT-NOSED CYLINDRICAL AFTERBODIES AT HYPERSONIC MACH NUMBERS

4. DESCRIPTIVE NOTES (Type of report and inclusive dates)

January 1961 to December 1966 - Final Report

5 AUTHOR(S) (First name, middle initial, last name)

R. H. Eaves, Jr., ARO, Inc.

6 REPORT DATE	7a. TOTAL NO. OF PAGES	7b. NO. OF REFS
May 1968	69	35

8a. CONTRACT OR GRANT NO.	9a. ORIGINATOR'S REPORT NUMBER(S)
AF 40(600)-1200	
b. PROJECT NO	AEDC-TR-68-82
c. Program Element 6540223F	9b. OTHER REPORT NO(S) (Any other numbers that may be assigned this report)
d.	N/A

10 DISTRIBUTION STATEMENT

This document has been approved for public release and sale; its distribution is unlimited.

11 SUPPLEMENTARY NOTES	12 SPONSORING MILITARY ACTIVITY
Available in DDC	Arnold Engineering Development Center, Air Force Systems Command Arnold Air Force Station, Tenn.

13 ABSTRACT

This study provides a readily solvable correlating equation that accurately predicts the pressure distribution over the afterbodies of various blunt-nosed cylinders at hypersonic Mach numbers. The correlating equation is developed from experimental pressure data on a cylinder with three nose shapes (hemisphere, flat-face, and rounded-shoulder flat-face) at free-stream Mach numbers of 6, 8, and 10. For blunt-nosed cylinders with nose drag coefficients from 0.89 to 1.72, the correlating equation is applicable over an extended experimental range of Mach number from 5.0 to 10.2 for local pressures greater than free-stream pressure. A good correlation is obtained with the method of characteristics solutions for Mach numbers from 5 to 100 for ten nose diameters along the body, but the applicability of the correlating equation beyond the experimental limits has not been demonstrated.

DD FORM 1 NOV 65 1473

Security Classification

14 KEY WORDS	LINK A		LINK B		LINK C	
	ROLE	WT	ROLE	WT	ROLE	WT
cylindrical afterbodies						
hypersonic flow						
pressure						
drag						
blunt-nosed cylinders						